NOMENCLATURE

Lower case

b	smallest distance between the crack boundary and the external surface of the fibre (mm)
r	inner crack radius (mm)

Upper case

F	force (mm)
GTN	Gurson-Tvergaard-Needleman model
K_I	stress intensity factor for fracture mode I ($MPam^{-1/2}$)
K_{Ic}	fracture toughness($MPam^{-1/2}$)
LEFM	linear elastic fracture mechanics
L_1	length 1 in the tensile specimen (mm)(see Figure 2)
L_2	length 2 in the tensile specimen (mm)(see Figure 2)
R_{min}	minimum specimen radius after the test (mm)
R_{out}	specimen radius outside the necking after the test (mm)
R	specimen radius (mm)

Greek

ϕ	diameter of the specimen
ε	strain
σ	stress
C_{ij}	coefficients defined in Table 5

STUDY OF THE LAST PART OF THE LOAD-DEFORMATION CURVE OF CONSTRUCTION STEELS WITH DISTINCT FRACTURE PATTERNS

Keywords: Tensile test, Load-deformation curve, Internal damage, Brittle-ductile transition.

Abstract. *The principal mechanical characteristics of construction steels are obtained by tensile testing. Nevertheless, the standards neglect the behaviour of steel beyond the maximum load point and do not define parameters related to the part of the load-deformation curve that lies between the maximum load point and failure. The necking process that begins when the maximum load is reached makes it somewhat difficult to study the material behaviour beyond that point. However, the ductility of steel is highly affected by this last part of the load-deformation curve. For such a reason, and especially since structural safety is directly related to ductility, a deeper knowledge of this may help in designing safer structures. In this paper, this part of the load-deformation curve is analysed in two construction steels that exhibit distinct fracture patterns: one shows the typical cup-cone fracture surface, while the other shows a flat fracture surface with a dark region inside. An experimental campaign has been carried out with cylindrical specimens of contrasting diameters: 3mm, 6mm and 9mm for each material. The use of a digital image correlation system is shown to be extremely useful in studying the behaviour of steel beyond the maximum load point, with an innovative procedure for identifying the growth of the internal damage that leads to failure in a specimen being developed.*

1.1 INTRODUCTION

The tensile test is the most commonly used such a test for characterising construction steels. It provides the load-deformation curve of a material up to the maximum load point, where the necking process begins and makes it difficult to obtain the last part of the curve. Due to these difficulties, the last part of the load-deformation curve is usually neglected.

Civil engineering structures, such as bridges and buildings, are projected by assuming that materials work elastically which may lead to the conclusion that deepening the knowledge of the plastic part of the load-deformation curve is unnecessary. Nevertheless, it has a strong influence on the structural safety of a building: if it is long, a structural element can be highly deformed before failure and, therefore, transmit some load to adjacent structural elements, which increases the energy absorbed by the structure before collapse.

In addition, the fracture of metallic materials is usually explained with the theory of nucleation, growth and coalescence of microvoids. This theory has given rise to several numerical models, such as the Gurson-Tvergaard-Needleman (GTN) model [1,2], which is based on the behaviour of an incompressible spherical volume with a spherical void inside, studied by Rice and Tracey [3]. These models have successfully reproduced the fracture of many metallic materials, which usually present the typical cup-cone fracture surface after being tested under tension. However, the cup-cone fracture surface is not the only possible fracture pattern. Another, for instance, involves eutectoid steel bars being used for manufacturing prestressing steel wires which, when tested under tension, reveal a highly different fracture surface that is flat, perpendicular to the loading direction and with a dark region in the centre of it.

This paper has two main objectives:

- The first involves the remaining uncertainties about the last part of the load-deformation curve. In order to study this, two construction steels are analysed, each of which presents a different fracture surface pattern: while one shows the typical cup-cone surface, the other reveals the aforementioned flat surface with a dark region in the centre of it. The load-deformation curves are obtained by using a digital image correlation system, with the resulting fracture surfaces being analysed by measuring and comparing the parameters that define the dimensions of each fracture surface pattern.

- The second entails analysis of the flat fracture surface pattern. The fracture behaviour of the eutectoid steel, which exhibits this kind of fracture surface, has been analysed by using an innovative procedure and by applying liquid nitrogen during the test. This flat fracture pattern has been studied under the hypothesis of quasi-brittle fracture, assuming that the dark region observed on the fracture surface has a similar effect to that of an internal crack.

1.2 MATERIALS

Two materials with different fracture behaviours have been considered in this study. A brief description of them is presented below.

- ***Material 1***

In the manufacturing process to obtain steel wires, raw eutectoid steel bars are cold-drawn, reducing their section by pulling them through a conical die. For this research, specimens were obtained from raw eutectoid steel bars (0.77%C) used for manufacturing prestressing steel wires, that is to say, as they had not been affected by cold-drawing the material was as isotropic as possible. Table 1 shows the chemical composition of this steel; more information on this material can be consulted in [4].

[Table 1]

The cylindrical specimens made with this material, when tested under tension, do not show the typical cup-cone fracture but a flat surface, perpendicular to the loading direction and with a dark circular region in the centre (see Figure 1a). This material was studied by the authors in [5] and its behaviour reproduced with success using a triaxiality-dependent cohesive model.

- ***Material 2***

This material is a low-carbon steel (<0.24%C), commonly used as reinforcement in concrete structures. In particular, this steel is defined as B 500 SD; that is to say, it is a weldable steel with special ductility characteristics and a yield strength higher than 500 N/mm^2. The chemical composition can be consulted in Table 2.

[Table 2]

In this case, cylindrical specimens tested under tension show the typical cup-cone fracture pattern (see Figure 1b).

[Figure 1]

2 STUDY ON THE LAST PART OF THE F-ϵ CURVE WITH TWO CONSTRUCTION STEELS WITH DISTINCT FRACTURE BEHAVIOURS

- ***Specimens***

The specimens are cylindrical and three different diameters are considered: 3mm, 6mm and 9mm. The dimensions of these specimens meet the requirements defined by UNE-EN ISO 6892 [6] and according to the parameters defined in Figure 2, are 20mm, 35mm and 50mm in the case of L_1 and 38mm, 53mm and 68mm in the case of L_2.for each diameter ϕ of, respectively, 3mm, 6mm and 9mm.

[Figure 2]

- ***Experimental procedure***

As mentioned in the introduction, the last part of the F-ε curve is usually neglected because the necking process makes it difficult to define. The use of a conventional extensometer presents two principal difficulties in this study: the first is that it does not generally allow valid information to be obtained after the maximum load point; the second is that it only allows information to be obtained for a specific initial gauge length. In order to avoid these problems, a digital image correlation system has been used. In Figure 3 a sketch of the experimental setup can be observed. With the use of a high-definition video camera, pictures

of the specimen throughout the test are obtained at a rate of one frame per second. Then, once the test is finished, the pictures are processed with a especially designed software and the strain is tracked between any two points of the specimen. Therefore, the deformation can be always tracked between points that are equally spaced from the fracture plane and the complete F-ε curve determined. In Figure 4 the results of a 3mm-diameter specimen tensile test obtained with both systems at the same time, a conventional extensometer and the digital image correlation system, can be seen. While the extensometer does not provide valid data from the maximum load point onward, the digital correlation system provides the same information as the extensometer up to that point and allows the complete F-ε curve to be obtained. More information on the validation of this procedure can be consulted in [7].

[Figure 3]

[Figure 4]

- ***Initial gauge length***

Since the use of a digital image correlation system allows different initial gage lengths to be used in the same test, three lengths have been considered:

- Initial gauge length equal to the specimen diameter (=1ϕ)
- Initial gauge length equal to twice the specimen diameter (=2ϕ)
- Initial gauge length equal to 12.5mm

- ***Results: σ-ε curves of Material 1 specimens***

Figures 5a, 5b and 5c show the σ-ε curves for the three initial gauge lengths considered. Since the last point of each curve cannot be distinguished in these figures, the last deformations measured for each test are plotted in Figures 6a, 6b and 6c.

[Figure 5]

[Figure 6]

The curves obtained for initial gauge lengths that are proportional to the specimen diameters (Figures 5a and 5b) seem to be highly repetitive for each of the three diameters considered. Regarding the last deformation measured in the specimens of different diameters, no increasing or decreasing pattern can be observed (see Figures 6a and 6b).

Nevertheless, in the curves obtained for an initial gauge length equal to 12.5mm, clear differences can be observed (Figure 5c). In fact, it appears that the higher the diameter, the higher is the last deformation measured (see Figure 6c). This is caused by the use of an initial gauge length of a constant value for different diameter specimens. Figure 7 shows the last picture obtained before failure in the three tests, one for each diameter considered. Over the profiles of the specimens, a white line represents the 12.5mm initial gauge length. This gauge length clearly covers the whole region affected by the necking process in the 3mm diameter specimen. While in the 6mm diameter specimen the region affected by the necking process is hardly covered, in the 9mm diameter specimen it is not completely covered. This explains the differences observed in the F-ε curves obtained with this gauge length and the increasing

pattern observed in Figure 6c, since the closer the fracture surface, the higher is the strain gradient. Therefore, use of an initial base of the same length for specimens of different diameters makes the results incomparable with each other.

[Figure 7]

- ***Results: σ-ε curves of Material 2 specimens***

Figures 8a, 8b and 8c show the σ-ε curves obtained for the three initial gauge lengths considered with the specimens of Material 2. The last deformations measured for each test are plotted in Figures 9a, 9b and 9c.

[Figure 8]

[Figure 9]

As in the case of the Material 1 specimens, σ-ε curves are highly repetitive for the initial gauge lengths that are proportional to the specimen diameters (Figures 8a and 8b). The last deformation measured for these gauge lengths is unaffected by the specimen diameter, as can be observed in Figures 9a and 9b. However, when a 12.5mm gauge length is used, the σ-ε curves present clear differences (see Figure 8c) and the last deformation measured seems to increase the value linearly with the specimen diameter (see Figure 9c). This, again, is the consequence of using a constant gauge length with specimens of different diameters.

- ***Results: geometrical analysis of the fracture surfaces***

In the fracture surfaces of the Material 1 specimens, a dark circular region can be identified. At first sight, it does not seem to be proportional to the specimen diameter. In order to study this point, the minimum diameter of the specimen at the end of the test (R_{min}) and the dark region diameter (r) have been measured for each specimen (see Figure 10a).

The Material 2 specimens show the typical cup-cone fracture surface. In this case, the dimensions measured are the minimum diameter of the specimen at the end of the test (R_{min}) and the diameter of the flat base of the cup-cone pattern (r) (see Figure 10b).

[Figure 10]

The results of these measurements can be observed in Tables 3 and 4. With r and R_{min}, as defined before, representing specimens of each material (see Figure 10), Figures 11 and 12 show how the r/R_{min} ratio modifies with R_{min}.

[Table 3]

[Table 4]

[Figure 11]

[Figure 12]

In the case of Material 2, the r/R_{min} ratio seems to be constant regardless of the specimen diameter. This means that the fracture surfaces are homothetic and that the fracture

mechanism seems to be unaffected by the specimen diameter. Nevertheless, in the case of Material 1, the r/R_{min} ratio seems to decrease for an increasing value of R_{min}.

3 ANALYSIS OF THE FLAT FRACTURE SURFACE PATTERN

- ***Hypothesis***

Since the r/R_{min} ratio does not present a constant value for different diameter specimens in the case of the Material 1 fracture pattern, the following hypothesis is proposed: although the material behaviour is ductile, the final fracture mechanism corresponds to that of a quasi-brittle behaviour. In this case, the dark region observed at the fracture surface would act as a crack developed during the test and would be responsible for the final fracture initiation. This assumption agrees with the results obtained in [5], where the fracture process of this material under a tensile test was modelled by means of a triaxiality-dependent cohesive model.

In order to check this hypothesis, two studies have been performed:

- A set of tests to verify if the dark region corresponds to an internal crack developed during the test.

- An analysis of the geometric parameters measured on the final fracture surfaces, using linear elastic fracture mechanics (LEFM) as a valid approach.

- ***Tests on embrittled specimens by use of liquid nitrogen***

The main purpose of the following experimental work is to verify that the dark region observed in the fracture surface corresponds to an internal crack developed before failure.

In this analysis, only 6mm diameter specimens were used, with the dimensions being the same as those in Figure 2. The procedure followed is described as follows:

1. A specimen is tested up to a specific deformational state and the test stopped before failure. Then, the specimen is unloaded. At the end of this first step, the internal damage may be present inside the material.

2. The specimen is embrittled by using liquid nitrogen and tested again until failure by applying a rapid displacement of the clamping jaws. If the material contains the internal damage developed in the first step, the fracture induced in this second step will take place in that section and will allow the damage that took place in the first step to be identified.

In order to check if the fracture induced by embrittling the material by use of liquid nitrogen induces a brittle fracture, a specimen was tested directly through application of the second step of this procedure. Figure 13 shows the fracture surface of this specimen and confirms that the second step of the procedure leads to brittle fracture, since no necking or the dark internal region can be observed (dark areas are shadows produced by the irregularities of the fracture surface).

[Figure 13]

Once the validity of this procedure was confirmed, a second specimen was tested up to a highly advanced deformational state and unloaded. Then, following the second step of the procedure, it was embrittled by using liquid nitrogen and tested up to failure. Figure 14 shows the fracture surface of the specimen, where a small dark region can be clearly identified.

In addition to this, before applying the second step of the procedure to the second specimen, it was analysed by using an X-ray computed tomography system (Nanotom 160NF, Phoenix). Figure 14 compares the result obtained with the tomography system and the fracture surface observed after applying the second step of the procedure. Both results confirm that internal damage grows inside the material during the test, showing a dark region placed in the same location of the cross section.

[Figure 14]

- ***Analysis of the flat fracture pattern by using an approach based on LEFM***

This analysis is developed by considering the dark region observed in the fracture surfaces of the Material 1 specimens as an internal crack. For this purpose, the formula defined by Guinea, Rojo and Elices has been used [8,9]. This allows the stress intensity factor to be obtained for a cylindrical fibre with an inner circular crack placed eccentrically, perpendicular to the longitudinal axis and under a tensile force applied along the longitudinal direction. This formula has the following expression:

$$\frac{K_I}{K_0} = 1 + \sum_{i=1}^{5} C_{i0} \left(\frac{r}{R} \right)^{\frac{2i+1}{2}} + \sum_{i=1}^{3} \left\{ Ln\left[1 + \left(\frac{r}{R} \right)^{2i} \right] \cdot \left[C_{i1} Ln^2 \left(\frac{b}{R} \frac{r}{R} \right) + \frac{C_{i2}}{\sqrt{\frac{b}{R} \frac{r}{R}}} \right] \right\}$$

with the reference stress intensity factor K_0 being defined as follows:

$$K_0 = \frac{2}{\pi} \sigma \sqrt{\pi \cdot r}$$

where:

K_{Ic}: stress intensity factor

b: smallest distance between the crack boundary and the external surface of the fibre

r: inner crack radius

R: fibre radius

σ: tensile stress applied

C_{ij}: coefficients defined in Table 5

[Table 5]

The meaning of these parameters can be consulted in Figure 15.

[Figure 15]

This expression relates the crack radius r, the specimen radius R and the dimension b to the stress intensity factor K_{Ic}. Therefore, considering as valid the values of R and b measured experimentally, an analytical value of r can be obtained by using this expression.

The value of K_{Ic} has been obtained by means of a three-point bending test by following the procedure defined by ASTM E 399-90 [10], resulting in 39MPa$\sqrt{}$m. R_{out} is the specimen radius outside the necking region and R_{min} is the minimum specimen radius after the test. Table 6 shows the values of R_{out}, R_{min}, b, r and the r/R_{min} ratio obtained experimentally, as well as the values of r and the r/R_{min} ratio obtained with the expression proposed by Guinea, Rojo and Elices.

[Table 6]

These results are plotted in Figure 16 and show how the values obtained with the expression proposed by Guinea, Rojo and Elices present the same pattern as those obtained experimentally. In both cases, although this pattern is more evident for the results obtained analytically, the r/R_{min} ratio tends to decrease when the specimen radius increases.

[Figure 16]

4 CONCLUSIONS

- Two steels with different failure behaviours have been analysed, with the first (Material 1) corresponding to steel used for manufacturing prestressing steel wires and the second (Material 2) corresponding to standard steel used as reinforcement in concrete structures.

- The use of a digital image correlation system allows the last part of the σ–ε curve to be obtained, between the maximum load point and failure, which is usually neglected even though it is of special interest from the structural safety point of view. Furthermore, this last part of the σ–ε curve seems to be highly repetitive even for different diameter specimens. These results can allow reconsideration of the deformation and stress at failure as additional parameters required by the Standards.

- An innovative procedure to detect internal damage in steel specimens has been offered by using liquid nitrogen to embrittle the material. This procedure has been checked by the use of X-ray computerised tomography.

- The cup-cone fracture surface, exhibited by the Material 2 specimens, appears to be homothetic between different diameter specimens while the flat surface exhibited by the Material 1 specimens does not. The analysis carried out by using an expression provided by LEFM would suggest that fracture mechanism of Material 1 may be considered as quasi-brittle.

ACKNOWLEDGEMENTS

The authors gratefully acknowledge the financial support provided for this research by the Spanish Ministerio de Economía y Competitividad under grant DPI 2011-24876. They also express their gratitude to Federico Sket and Jon M. Molina-Aldareguia, from IMDEA Materiales, for their support with providing the X-ray computerised tomographic system. Fernando Suárez also wishes to express his gratitude to the Fundación Agustín de Betancourt for the grant provided.

REFERENCES

[1] Gurson, A.L.: Continuum Theory of Ductile Rupture by Void Nucleation and Growth: Part I – Yield Criteria and Flow Rules for Porous Ductile Media, *J. Eng. Mater. Tech.* (January 1977)

[2] Tvergaard, V., Needleman, A., Analysis of the cup-cone fracture in a round tensile bar, *Acta metall.* Vol. 32, No. 1, pp. 157-169 (1984).

[3] Rice, J.R., Tracey, D.M., On the ductile enlargement of voids in triaxial stress fields. *Journal of the Mechanics and Physics of Solids*, vol. 17, nº3, pp 201-217 (1969)

[4] Atienza, J.M., Tensiones residuales en alambres de acero trefilados, PhD thesis, Universidad Politécnica de Madrid (2001)

[5] Suárez, F., Gálvez, J.C., Cendón D.A., Atienza, J.M., Fracture of eutectoid Steel bars under tensile loading: Experimental results and numerical simulation. *Engng Fract Mech* (2016)

[6] ISO 6892-1:2009, Metallic materials. Tensile testing. Part 1: Method of test at room temperature.

[7] Suárez, F., Estudio de la rotura en barras de acero. Aspectos experimentales y numéricos, PhD thesis, Universidad Politécnica de Madrid (2013)

[8] Guinea, G.V., Rojo, F.J., Elices, M., Stress intensity factors for internal circular cracks in fibers under tensile loading. Engineering Fracture Mechanics, vol. 71, nº3 pp. 365-377 (2004)

[9] Rojo, F., Aplicación de la mecánica de la fractura a la rotura frágil de fibras de sémola, PhD thesis, Universidad Politécnica de Madrid (2013)

[10] ASTM E 399-90, Standard Test Method for Plane-Strain Fracture Toughness of Metallic Materials (2003)

Table 1

Chemical composition of Material 1

C (%)	Si (%)	Mn (%)	P (%)	S (%)	Cr (%)	Mo (%)	Ni (%)	Cu (%)	Al (%)	Ti (%)	Nb (%)	V (%)	N (%)
0.83	0.25	0.72	0.012	0.004	0.24	<0.01	0.02	0.01	<0.003	<0.005	<0.005	<0.01	0.0097

Table 2

Chemical composition of Material 2

C (%)	Si (%)	Mn (%)	P (%)	S (%)	Cr (%)	Mo (%)	Ni (%)	Cu (%)	Al (%)	Ti (%)	Nb (%)	V (%)	N (%)
0.22	0.18	1.00	0.024	0.042	0.08	0.03	0.14	0.46	<0.003	<0.005	<0.005	<0.01	0.0113

Table 3

Geometric parameters measured on fracture surfaces of the Material 1 specimens.

Specimen	r (mm)	R_{min} (mm)	r/R_{min}
D3cp08	0.73	1.22	0.60
D3cp10	0.71	1.22	0.58
D3cp11	0.75	1.24	0.61
D6c0p16	0.97	2.32	0.42
D6c0p17	0.96	2.30	0.42
D6c0p18	0.97	2.33	0.42
D6c0p01_I	1.13	2.46	0.46
D6c0p02_I	1.15	2.42	0.47
D6c0p03_I	0.94	2.28	0.41
D6c0p01_II	0.97	2.32	0.42
D6c0p02_II	0.98	2.36	0.42
D6c0p03_II	0.97	2.29	0.42
D6c0p01_III	0.97	2.36	0.41
D6c0p02_III	1.01	2.36	0.43
D6c0p03_III	0.99	2.34	0.42
D9c0p04	1.44	3.70	0.39
D9c0p05	1.65	3.76	0.44
D9c0p06	1.54	3.82	0.40

Table 4

Geometric parameters measured on fracture surfaces of the Material 2 specimens.

Specimen	r (mm)	R_{min} (mm)	r/R_{min}
Ar3c0p01	0.54	0.88	0.61
Ar3c0p02	0.57	0.89	0.64
Ar3c0p03	0.56	0.92	0.61
Ar3c0p04	0.59	0.88	0.66
Ar3c0p06	0.55	0.88	0.63
Ar6c0p01	1.09	1.78	0.61
Ar6c0p02	1.14	1.84	0.62
Ar6c0p03	1.10	1.82	0.60
Ar9c0p01	1.66	2.78	0.60
Ar9c0p02	1.71	2.75	0.62
Ar9c0p03	1.66	2.80	0.59

Table 5

Coefficients used in the expression proposed by Guinea, Rojo and Elices [8].

	C_{i0}	C_{i1}	C_{i2}
i=1	0.01242	-0.3097	1.185
i=2	-6.388	1.547	-3.723
i=3	16.89	-0.8769	2.628
i=4	-9.838	---	---
i=5	-1.228	---	---

Table 6

Comparison between the experimental measurements and those obtained with the expression proposed by Guinea, Rojo and Elices [8, 9] for Material 1.

	R_{out} (mm)	R_{min} (mm)	b (mm)	r (mm)		r/R_{min}	
				Measured	Guinea-Rojo-Elices	Measured	Guinea-Rojo-Elices
D3c0p08	1.46	1.22	0.24	0.73	0.74	0.60	0.61
D3c0p10	1.45	1.22	0.28	0.71	0.77	0.58	0.62
D3c0p11	1.47	1.24	0.35	0.75	0.80	0.61	0.65
D6c0p16	2.90	2.32	1.19	0.97	1.07	0.42	0.46
D6c0p17	2.90	2.30	1.23	0.96	1.07	0.42	0.47
D6c0p18	2.92	2.33	1.13	0.97	1.07	0.42	0.46
D6c0p01_I	2.92	2.46	1.08	1.13	1.06	0.46	0.43
D6c0p02_I	2.93	2.42	1.11	1.15	1.06	0.47	0.44
D6c0p03_I	2.93	2.28	1.22	0.94	1.07	0.41	0.47
D6c0p01_II	2.93	2.32	1.14	0.97	1.07	0.42	0.46
D6c0p02_II	2.93	2.36	1.19	0.98	1.07	0.42	0.45
D6c0p03_II	2.94	2.29	1.00	0.97	1.05	0.42	0.46
D6c0p01_III	2.94	2.36	1.18	0.97	1.07	0.41	0.45
D6c0p02_III	2.95	2.36	1.20	1.01	1.07	0.43	0.45
D6c0p03_III	2.92	2.34	1.20	0.99	1.07	0.42	0.46
D9c0p04	4.35	3.70	1.91	1.44	1.13	0.39	0.31
D9c0p05	4.35	3.76	1.60	1.65	1.12	0.44	0.30
D9c0p06	4.38	3.82	1.62	1.54	1.12	0.40	0.29

FIGURE CAPTIONS

Figure 1: Fracture surfaces of the materials tested: a) Material 1: flat fracture surface; b) Material 2: cup-cone fracture surface.

Figure 2: Specimen dimensions.

Figure 3: Sketch of the experimental setup used for measuring the deformation with a digital image correlation system.

Figure 4: F-ε curves in a tensile test obtained with a conventional extensometer and with a digital image correlation system. The former stops obtaining valid data when F_{max} is reached while the latter provides the complete F-ε curve.

Figure 5: σ–ε curves obtained with 3mm, 6mm and 9mm diameter specimens of Material 1: a) using an initial gauge length of 1ϕ; b) using an initial gauge length of 2ϕ;. c) using an initial gauge length of 12.5mm

Figure 6: ε_{rot} obtained with 3mm, 6mm and 9mm diameter specimens of Material 1: a) using an initial gauge length of 1ϕ; b) using an initial gauge length of 2ϕ;. c) using an initial gauge length of 12.5mm

Figure 7: Pictures of 3mm, 6mm and 9mm diameter specimens immediately before failure. For comparison, a 12.5mm gauge length is shown in white over each of them.

Figure 8: σ–ε curves obtained with 3mm, 6mm and 9mm diameter specimens of Material 2: a) using an initial gauge length of 1ϕ; b) using an initial gauge length of 2ϕ;. c) using an initial gauge length of 12.5mm

Figure 9: ε_{rot} obtained with 3mm, 6mm and 9mm diameter specimens of Material 2: a) using an initial gauge length of 1ϕ; b) using an initial gauge length of 2ϕ;. c) using an initial gauge length of 12.5mm

Figure 10: Geometric parameters measured on the fracture surfaces of the Material 1 specimens (a) and the Material 2 specimens (b)

Figure 11: r/R_{min} ratio for different diameter specimens of Material 1.

Figure 12: r/R_{min} ratio for different diameter specimens of Material 2.

Figure 13: Fracture surface obtained with a 6mm diameter specimen tested at low temperature by means of liquid nitrogen.

Figure 14: Fracture surface obtained with a 6mm diameter specimen tested initially up to an advanced deformational state and finally at low temperature by means of liquid nitrogen. The result obtained with an X-ray tomography system with the predeformed specimen is shown on the right.

Figure 15: Parameters used in the expression proposed by Guinea, Rojo and Elices [8,9] for Material 1.

Figure 16: r/R_{min} ratios measured experimentally compared with those obtained through the expression proposed by Guinea, Rojo and Elices [8,9] for Material 1.

.

Figure 1a

Click here to download high resolution image

Figure 1b
Click here to download high resolution image

Figure 2

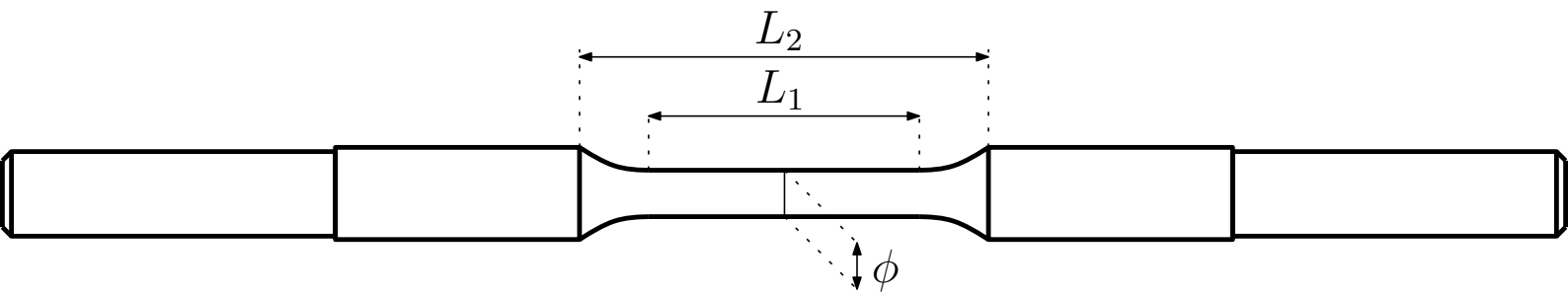

Figure 3
Click here to download high resolution image

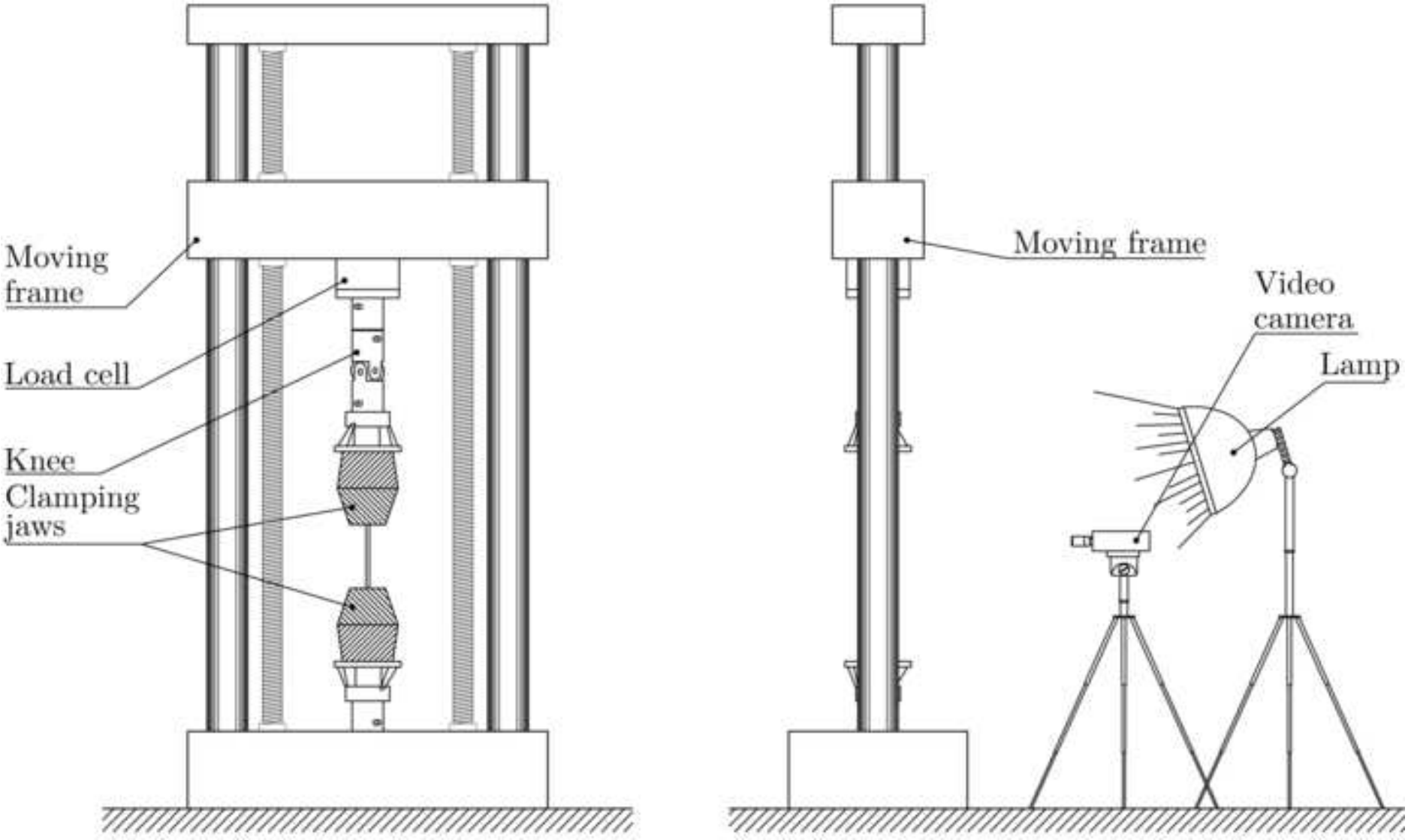

Figure 4

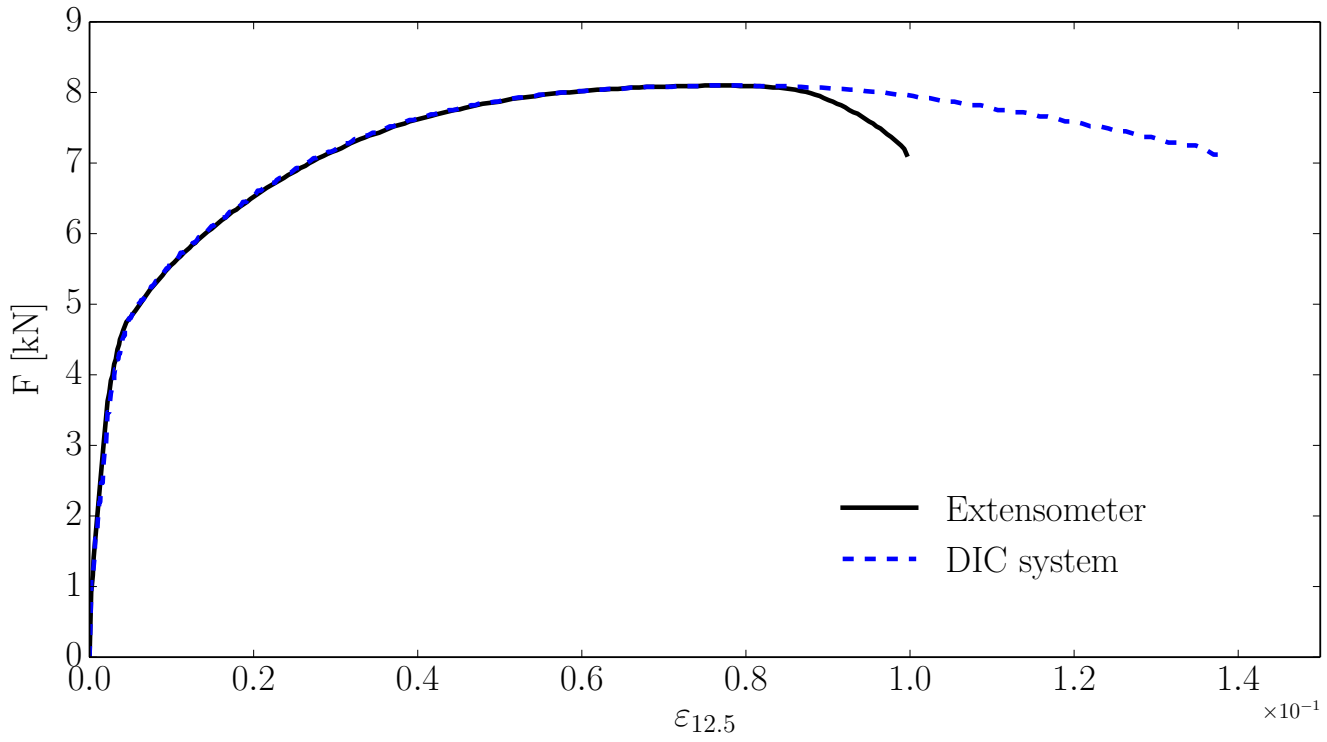
F [kN]
0
1
2
3
4
5
6
7
8
9
0.0
0.2
0.4
0.6
0.8
1.0
1.2
1.4
$\varepsilon_{12.5}$
$\times 10^{-1}$
Extensometer
DIC system

Figure 5a

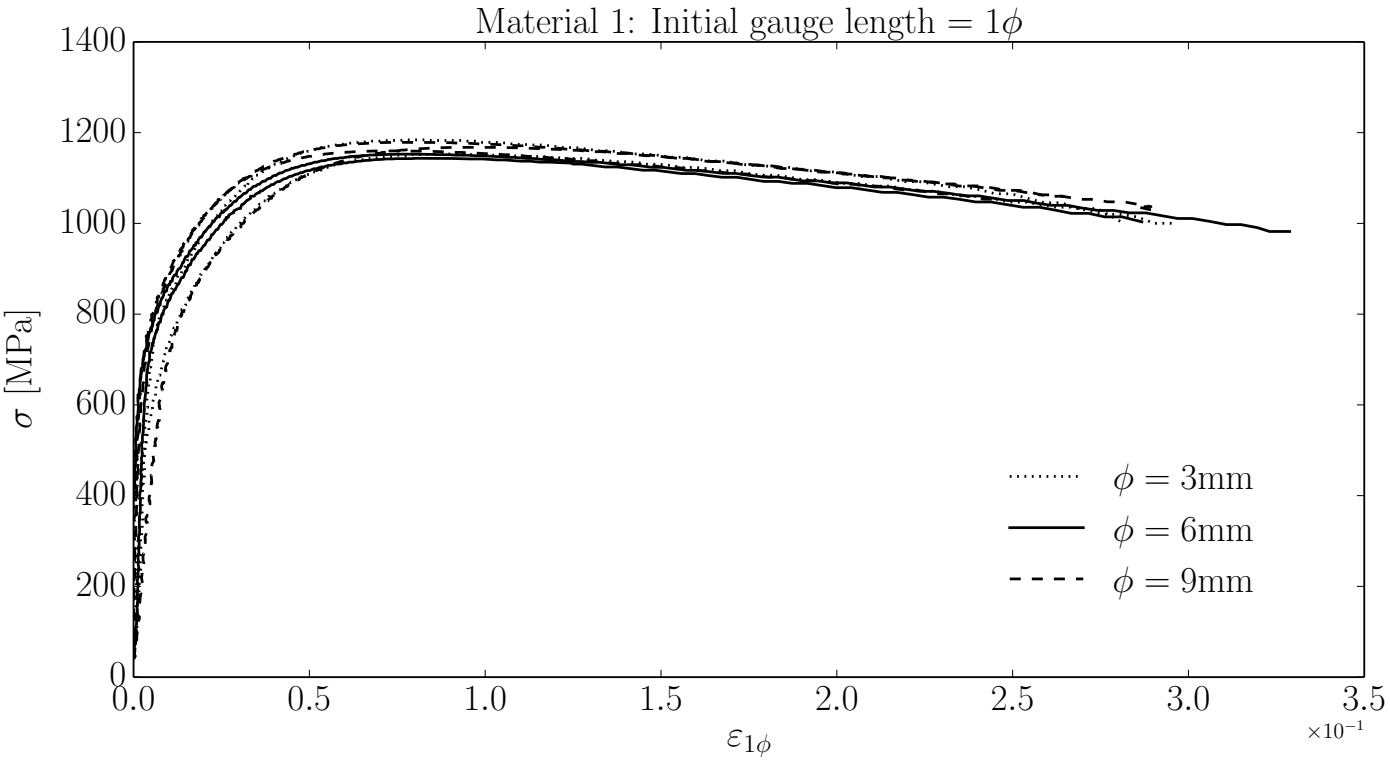
Material 1: Initial gauge length = 1ϕ
1400
1200
1000
800
600
400
200
0
σ [MPa]
0.0
0.5
1.0
1.5
2.0
2.5
3.0
3.5
$\times 10^{-1}$
$\varepsilon_{1\phi}$
$\phi = 3$mm
$\phi = 6$mm
$\phi = 9$mm

Figure 5b

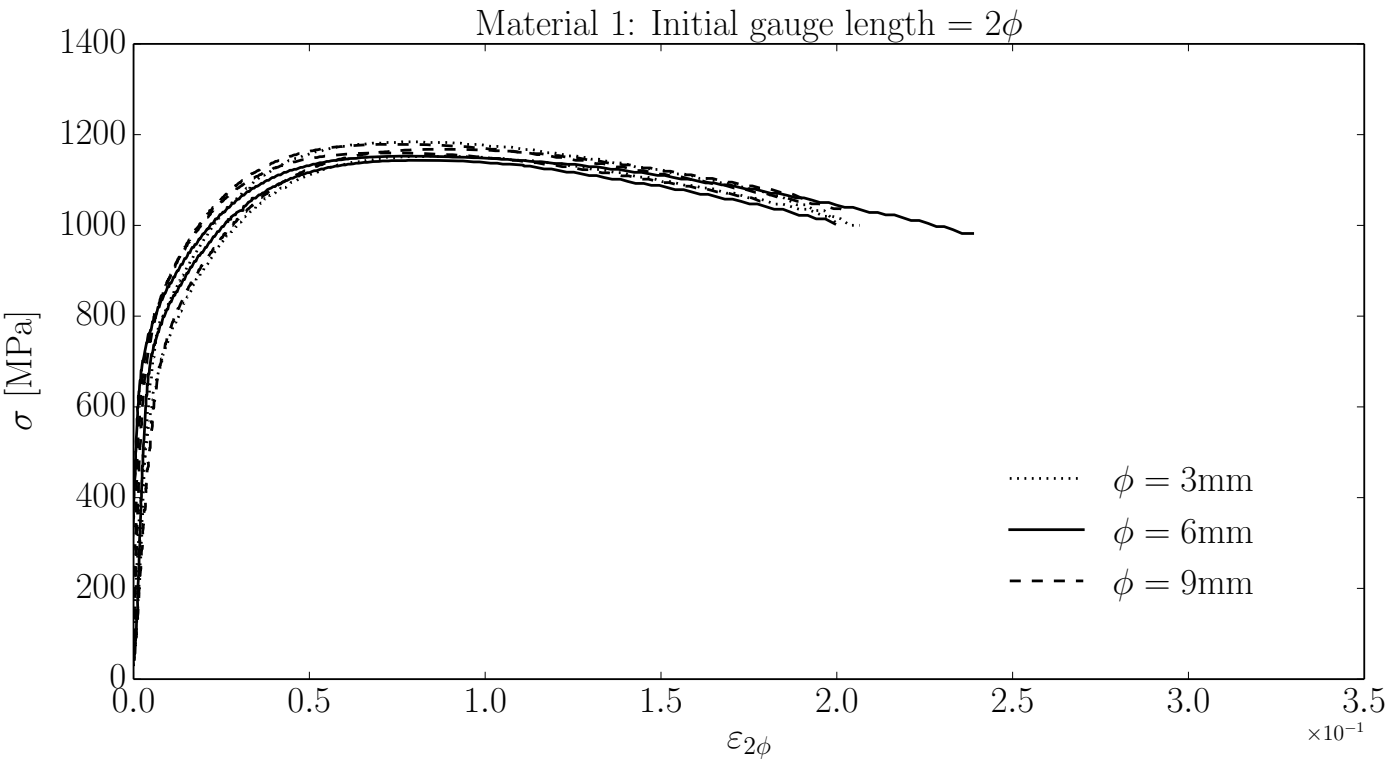
Material 1: Initial gauge length = 2ϕ
1400
1200
1000
800
600
400
200
0
σ [MPa]
0.0
0.5
1.0
1.5
2.0
2.5
3.0
3.5
$\times 10^{-1}$
$\varepsilon_{2\phi}$
$\phi = 3$mm
$\phi = 6$mm
$\phi = 9$mm

Figure 5c

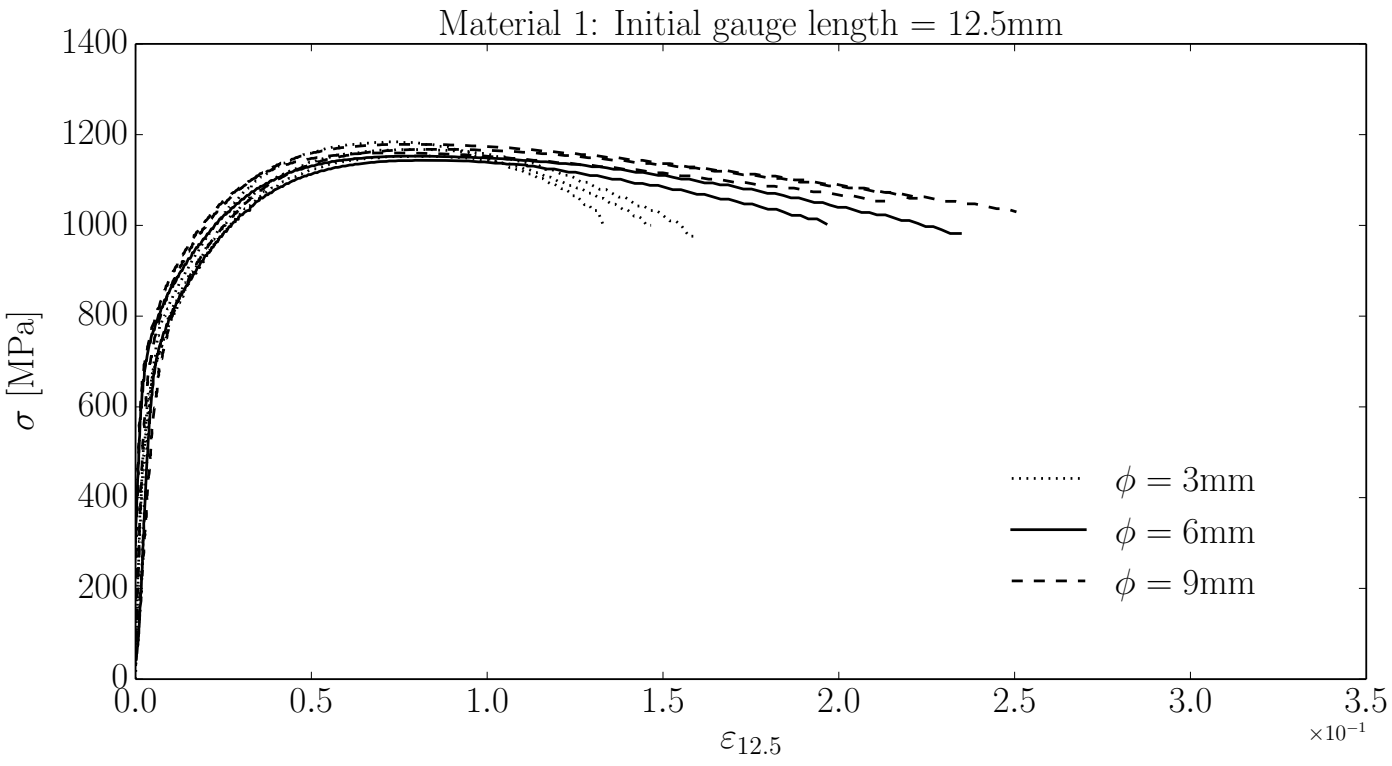
Material 1: Initial gauge length = 12.5mm
1400
1200
1000
800
600
400
200
0
σ [MPa]
0.0
0.5
1.0
1.5
2.0
2.5
3.0
3.5
×10⁻¹
ε12.5
ϕ = 3mm
ϕ = 6mm
ϕ = 9mm

Figure 6a

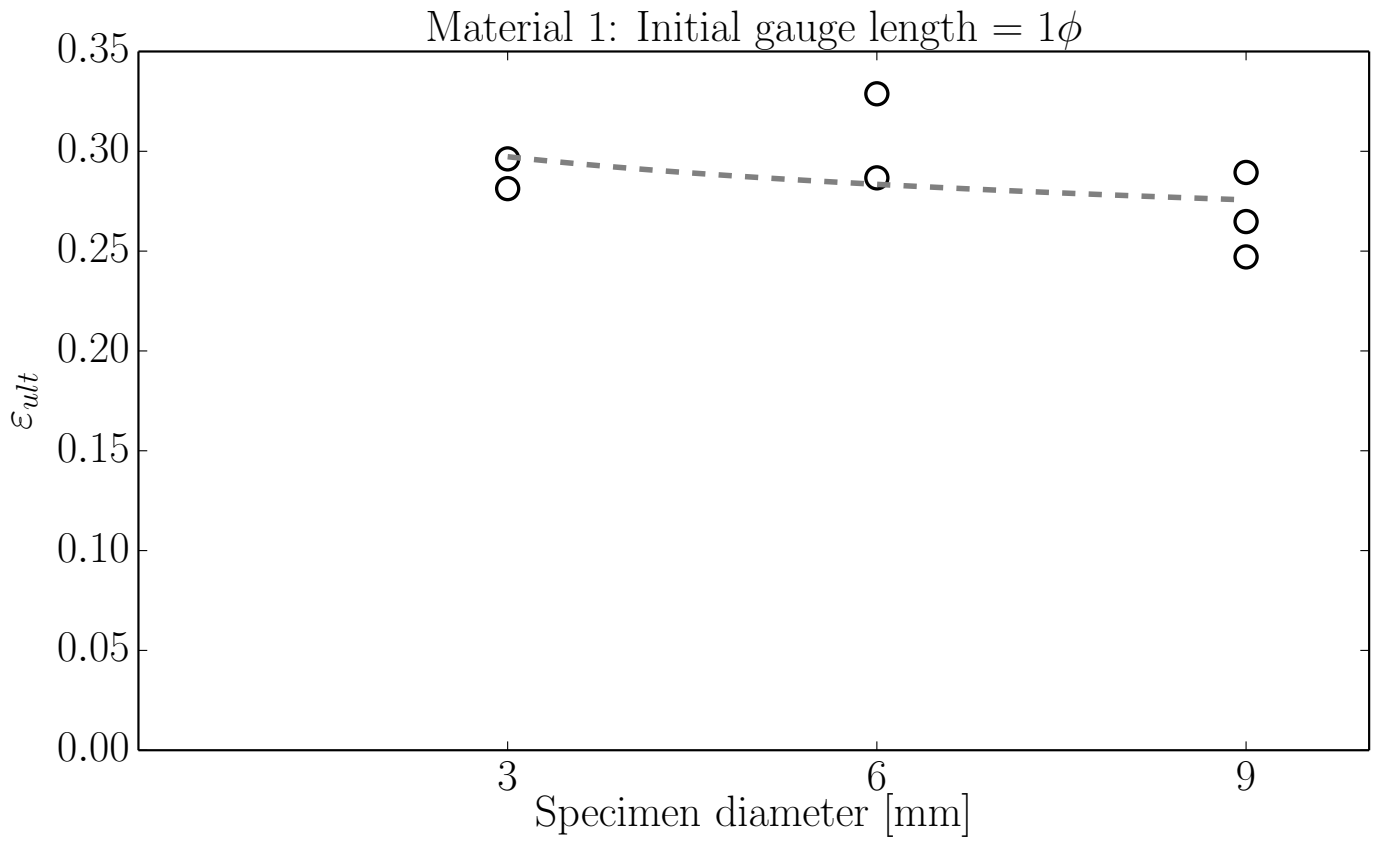
Material 1: Initial gauge length = 1ϕ
0.35
0.30
0.25
0.20
0.15
0.10
0.05
0.00
ε_{ult}
3
6
9
Specimen diameter [mm]

Figure 6b

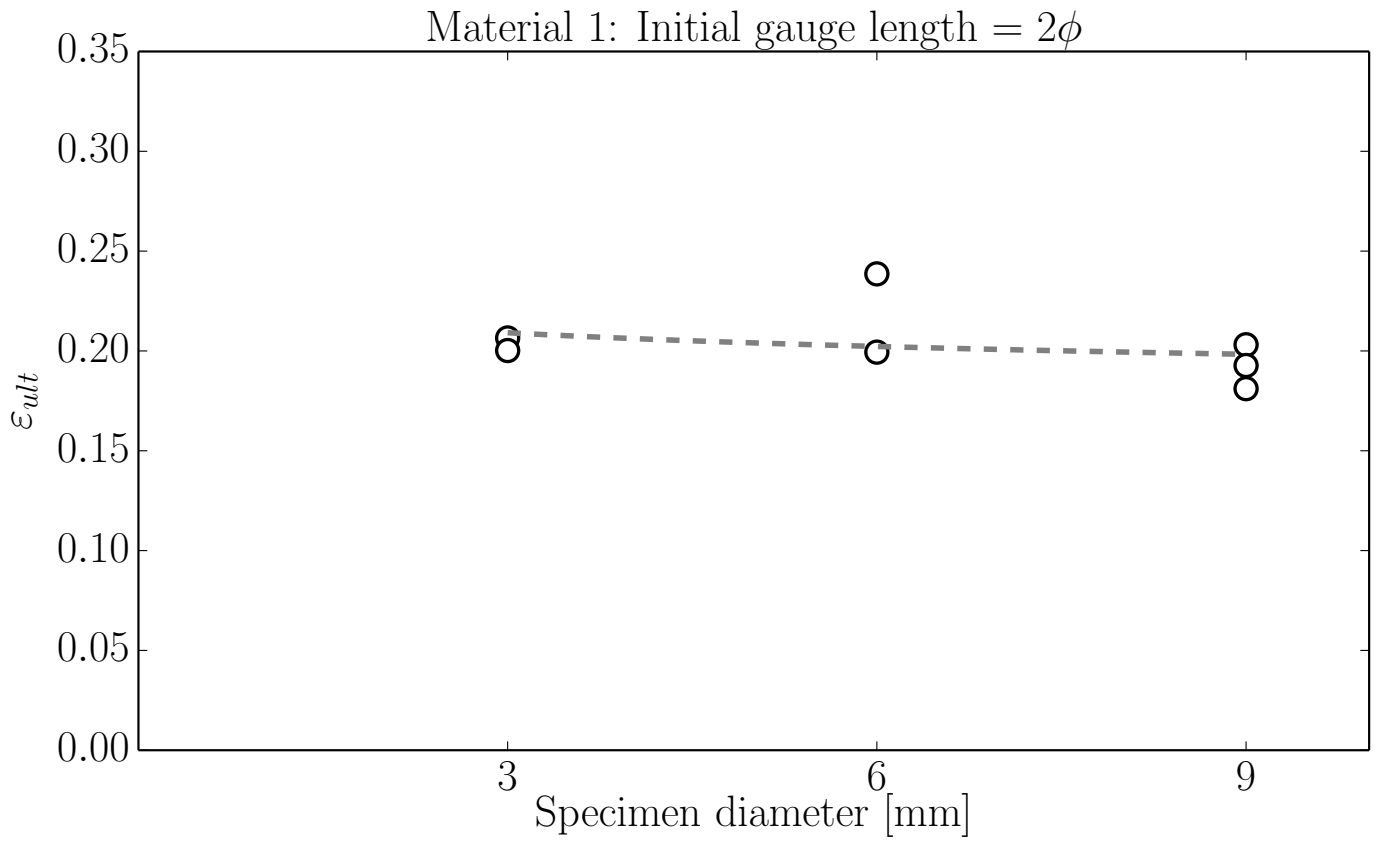
Material 1: Initial gauge length = 2ϕ
0.35
0.30
0.25
0.20
0.15
0.10
0.05
0.00
ε_{ult}
3
6
9
Specimen diameter [mm]

Figure 6c

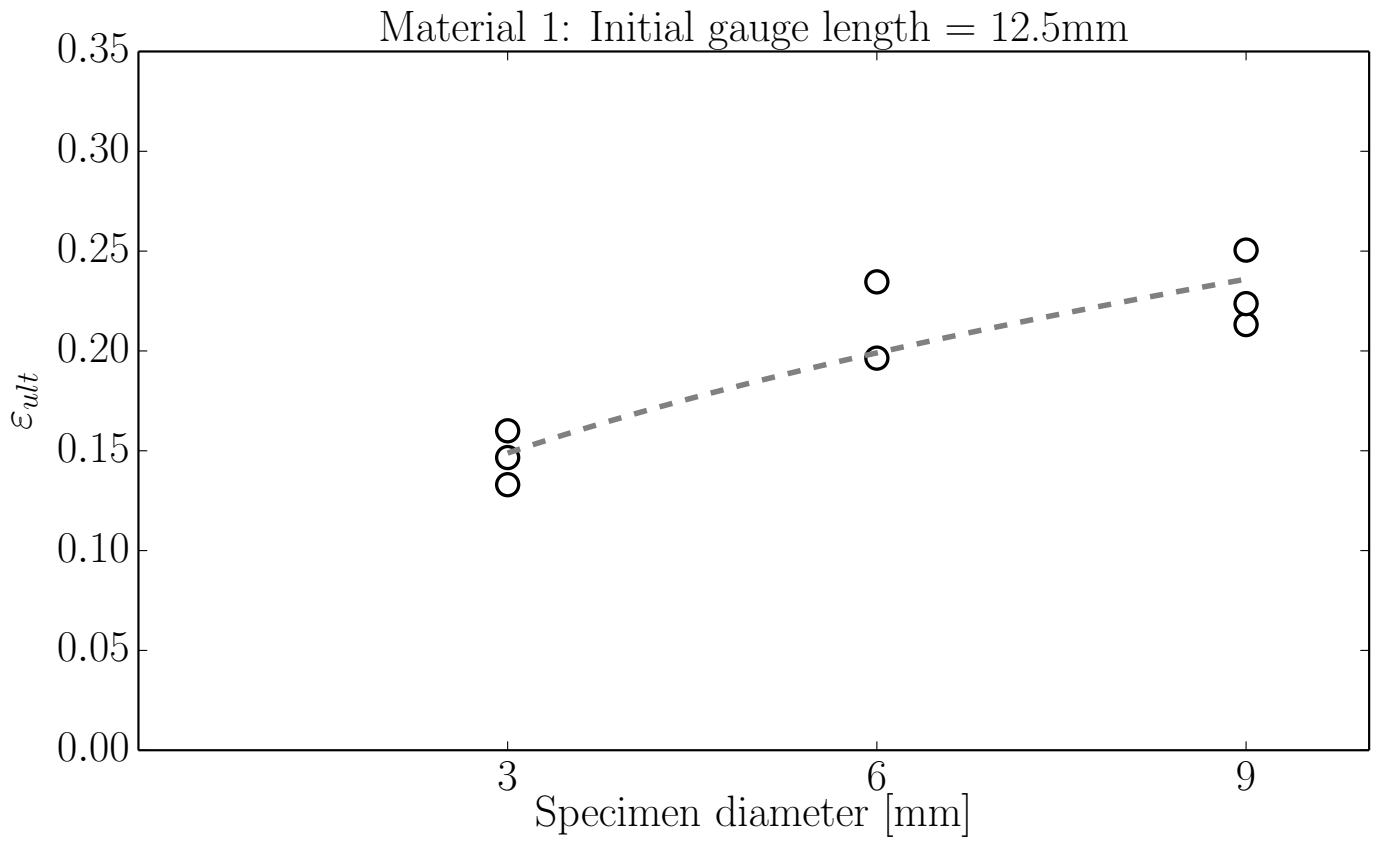
Material 1: Initial gauge length = 12.5mm
0.35
0.30
0.25
0.20
0.15
0.10
0.05
0.00
ε_{ult}
3
6
9
Specimen diameter [mm]

Figure 7

Click here to download high resolution image

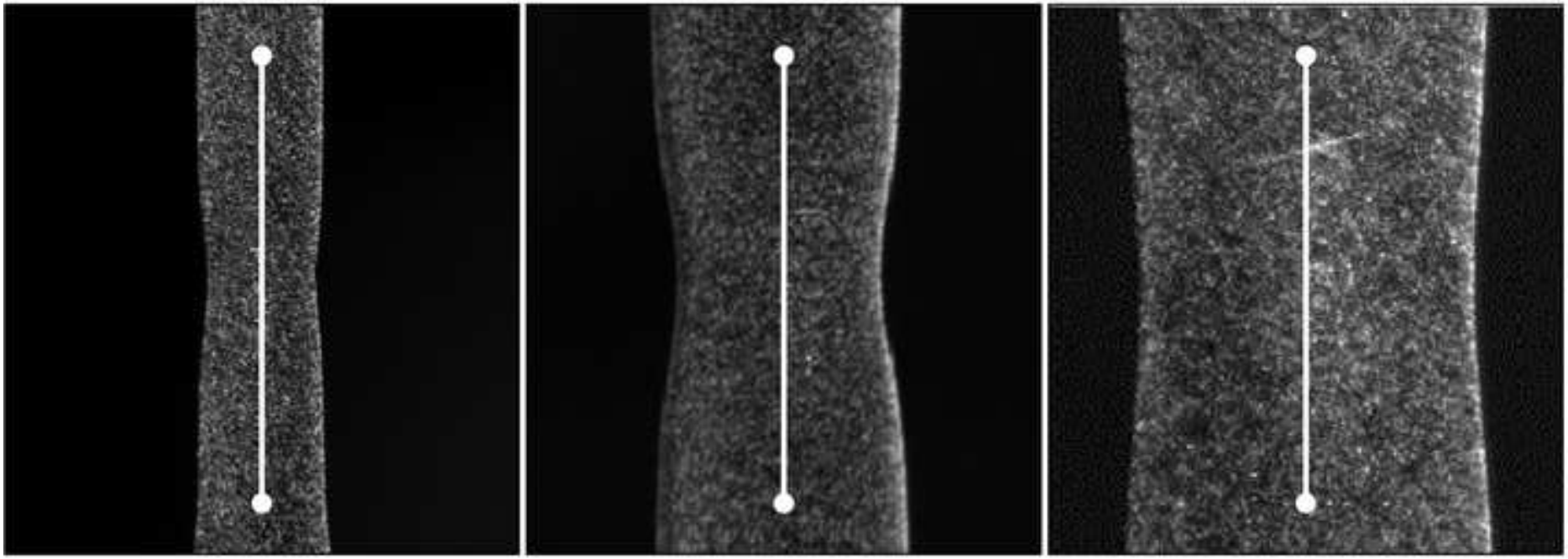

Figure 8a

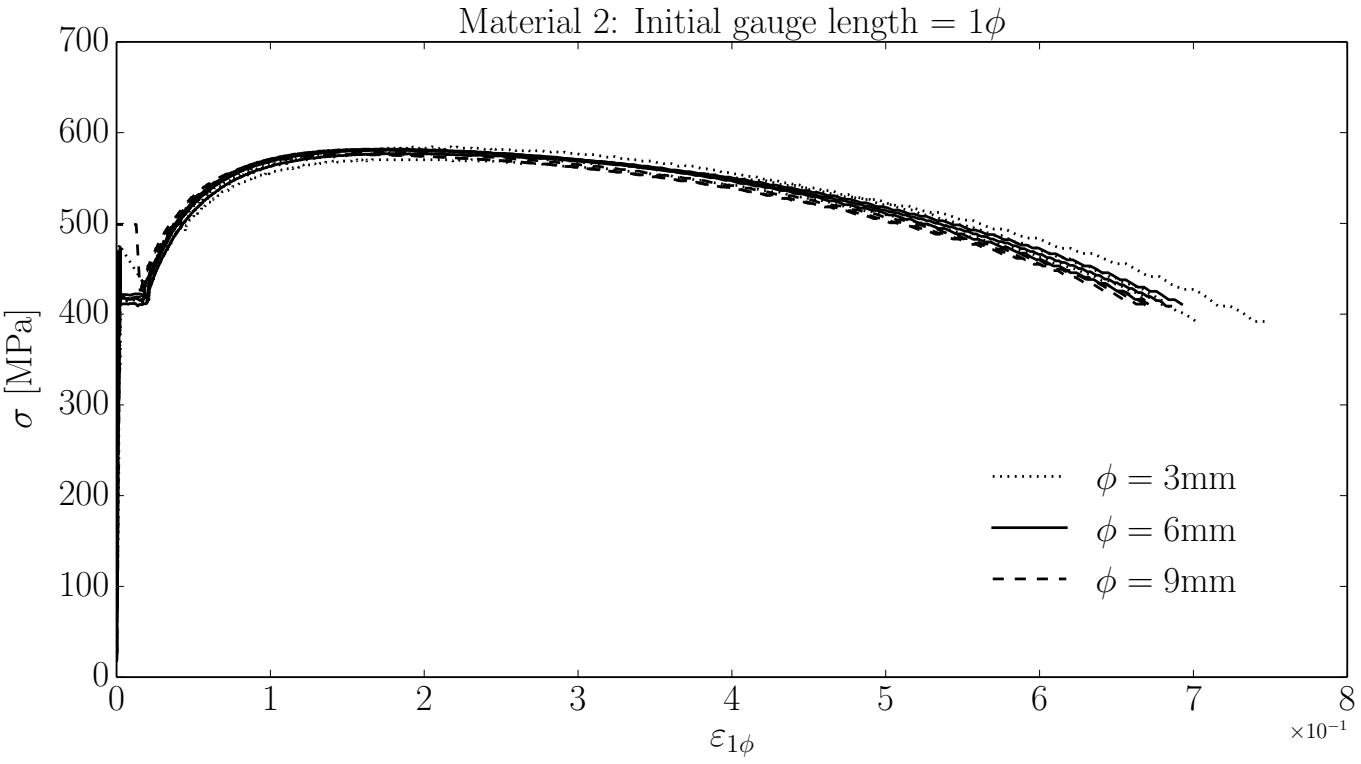
Material 2: Initial gauge length = 1ϕ
σ [MPa]
$\varepsilon_{1\phi}$
$\times 10^{-1}$
$\phi = 3$mm
$\phi = 6$mm
$\phi = 9$mm
0
100
200
300
400
500
600
700
0
1
2
3
4
5
6
7
8

Figure 8b

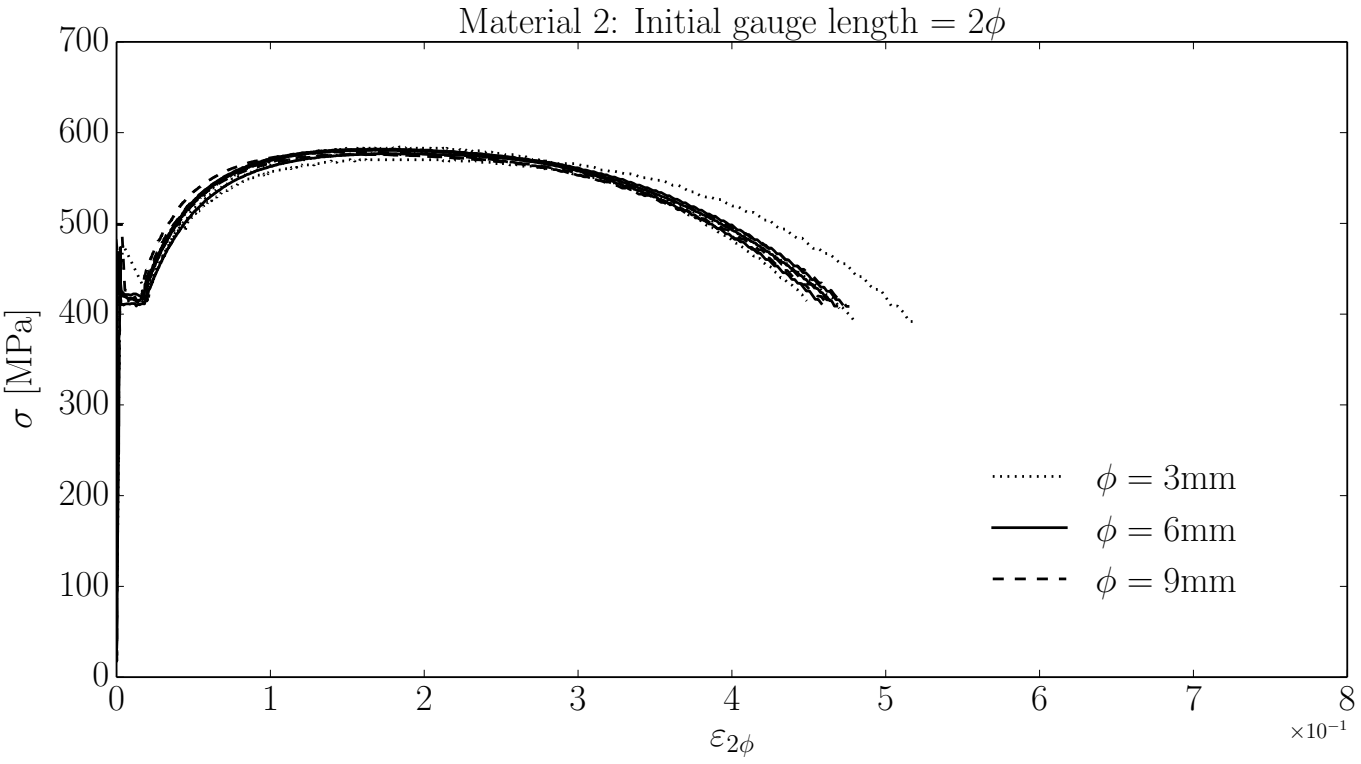
Material 2: Initial gauge length = 2ϕ
700
600
500
400
300
200
100
0
σ [MPa]
0
1
2
3
4
5
6
7
8
$\times 10^{-1}$
$\varepsilon_{2\phi}$
$\phi = 3$mm
$\phi = 6$mm
$\phi = 9$mm

Figure 8c

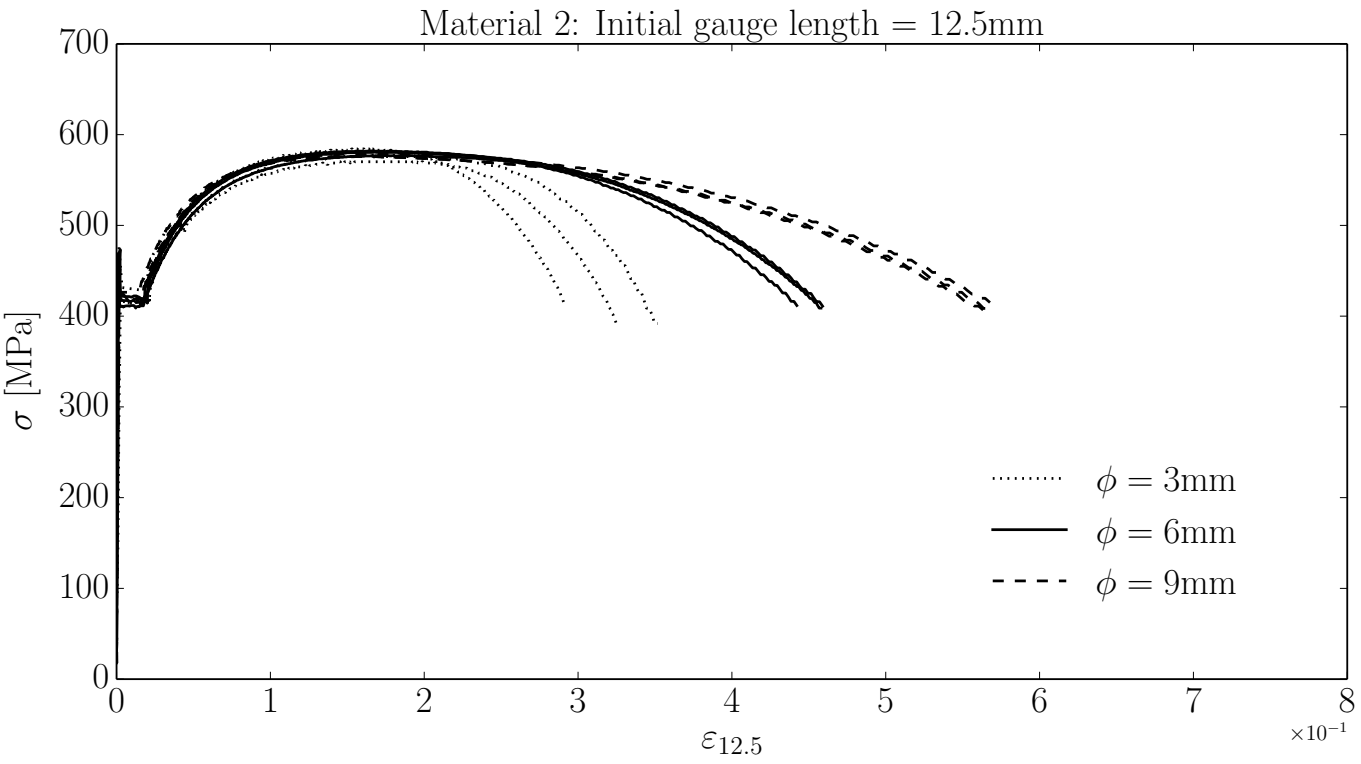
Material 2: Initial gauge length = 12.5mm
σ [MPa]
$\varepsilon_{12.5}$
×10⁻¹
$\phi = 3$mm
$\phi = 6$mm
$\phi = 9$mm

Figure 9a

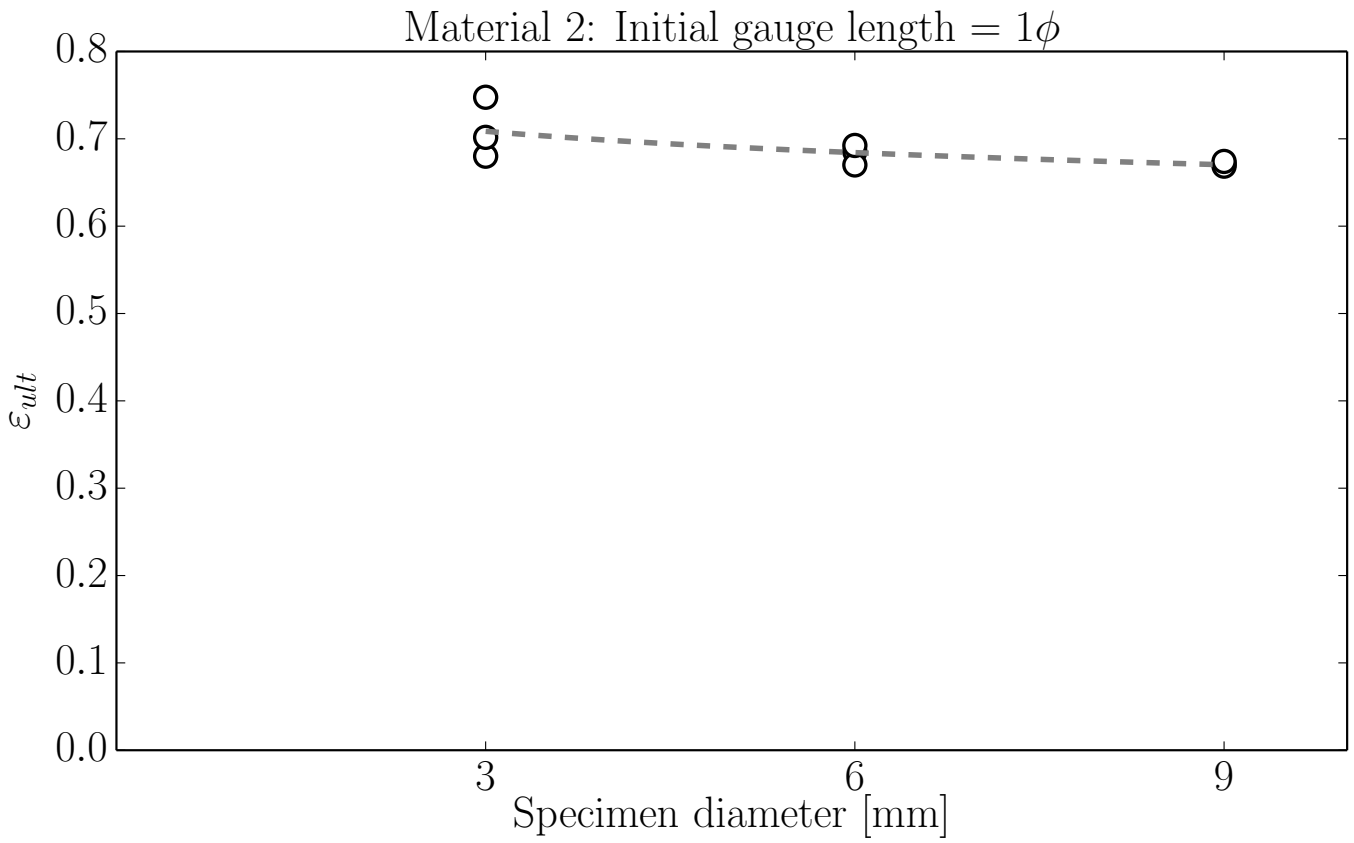
Material 2: Initial gauge length = 1ϕ
0.8
0.7
0.6
0.5
0.4
0.3
0.2
0.1
0.0
ε_{ult}
3
6
9
Specimen diameter [mm]

Figure 9b

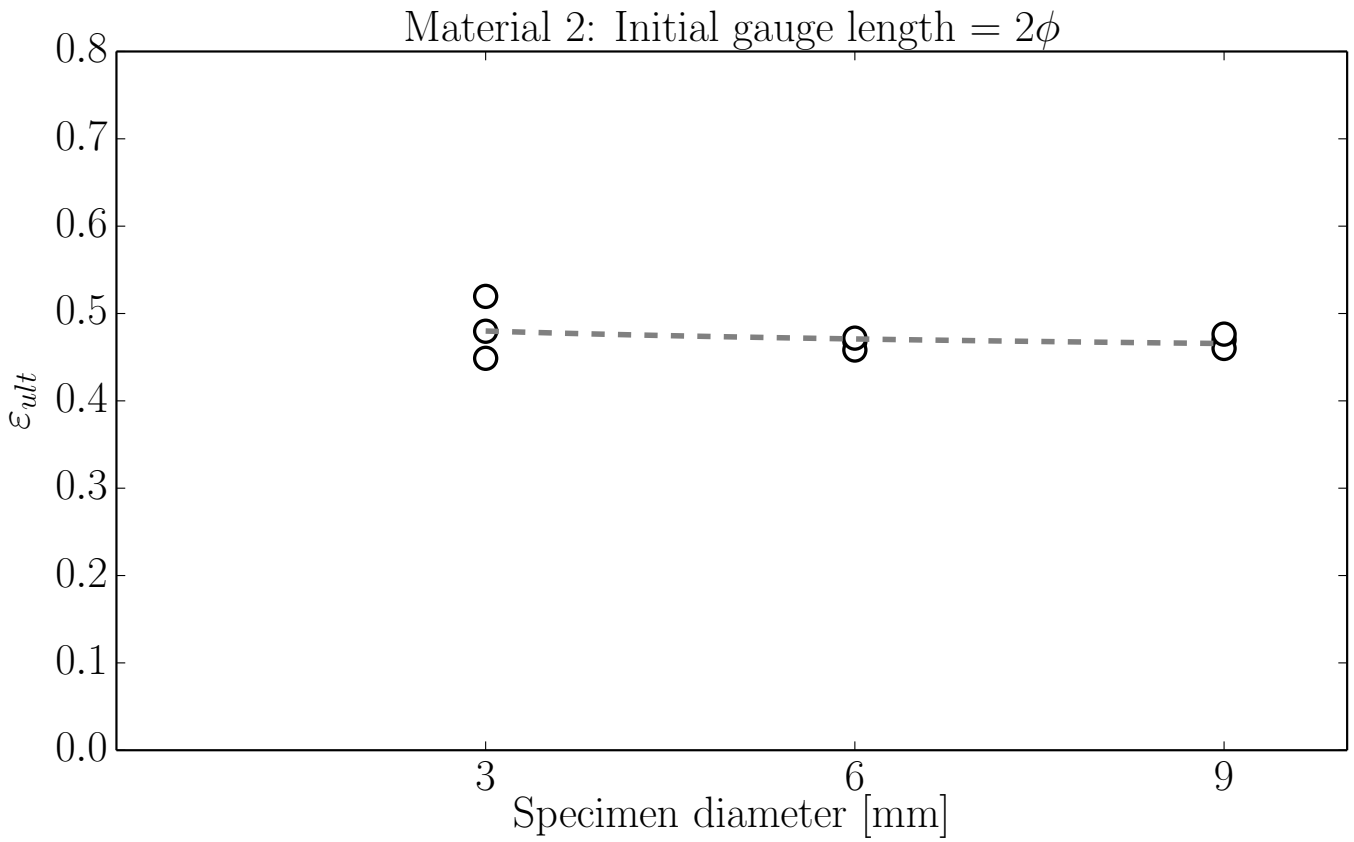
Material 2: Initial gauge length = 2ϕ
0.8
0.7
0.6
0.5
0.4
0.3
0.2
0.1
0.0
ε_{ult}
3
6
9
Specimen diameter [mm]

Figure 9c

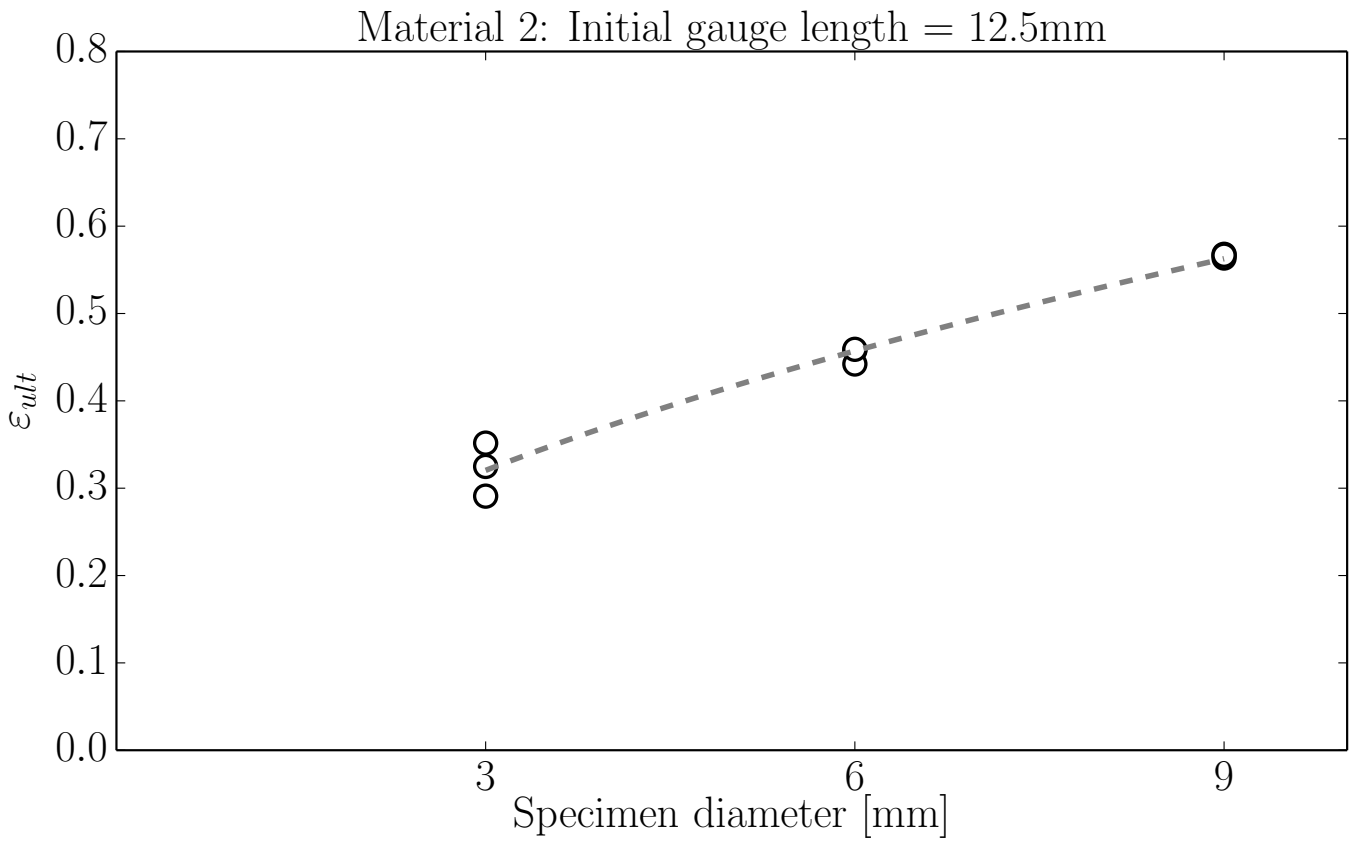
Material 2: Initial gauge length = 12.5mm
0.8
0.7
0.6
0.5
0.4
0.3
0.2
0.1
0.0
ε_{ult}
3
6
9
Specimen diameter [mm]

Figure 10a
Click here to download high resolution image

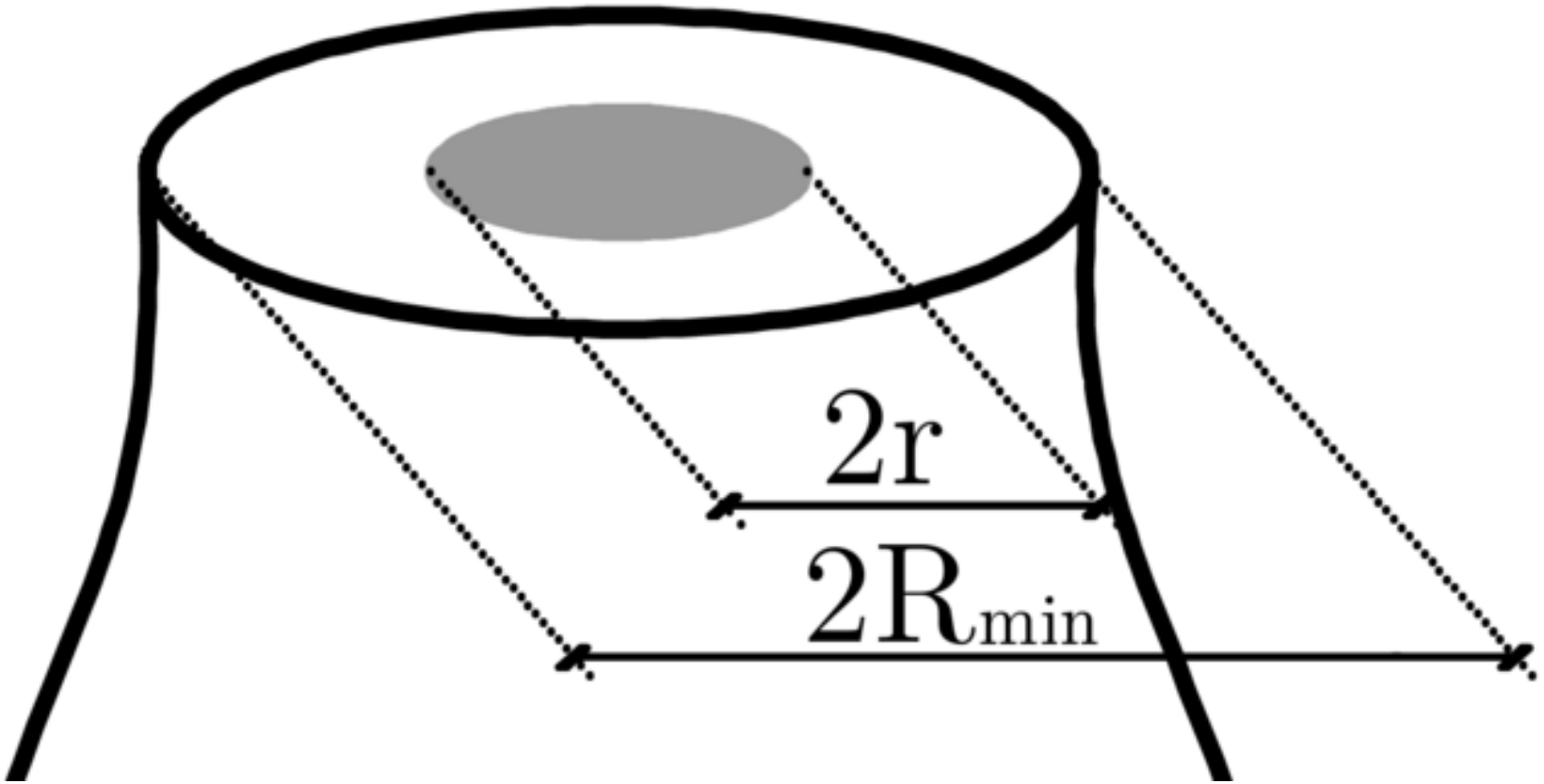

Figure 10b
Click here to download high resolution image

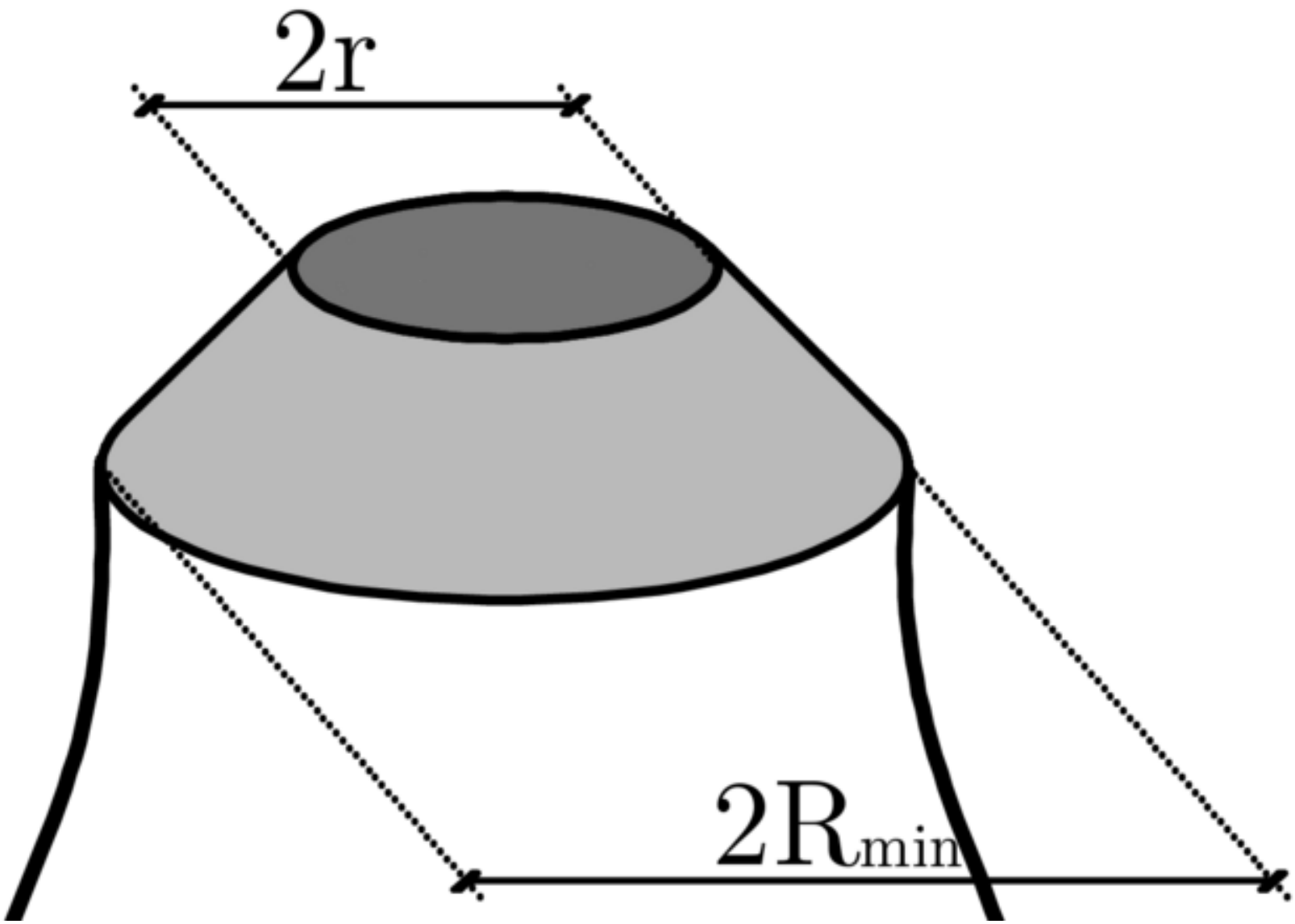

Figure 11

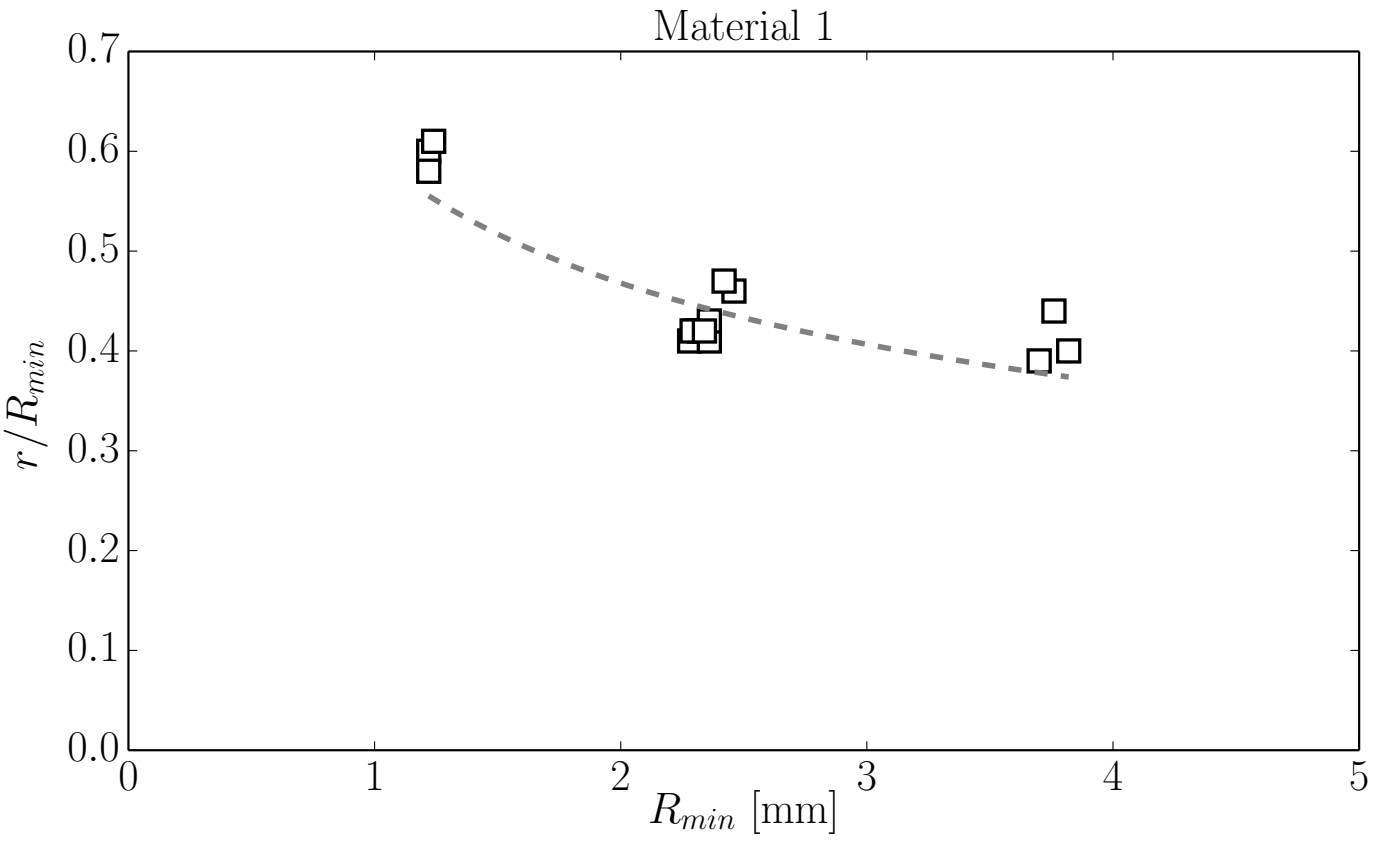

Figure 12

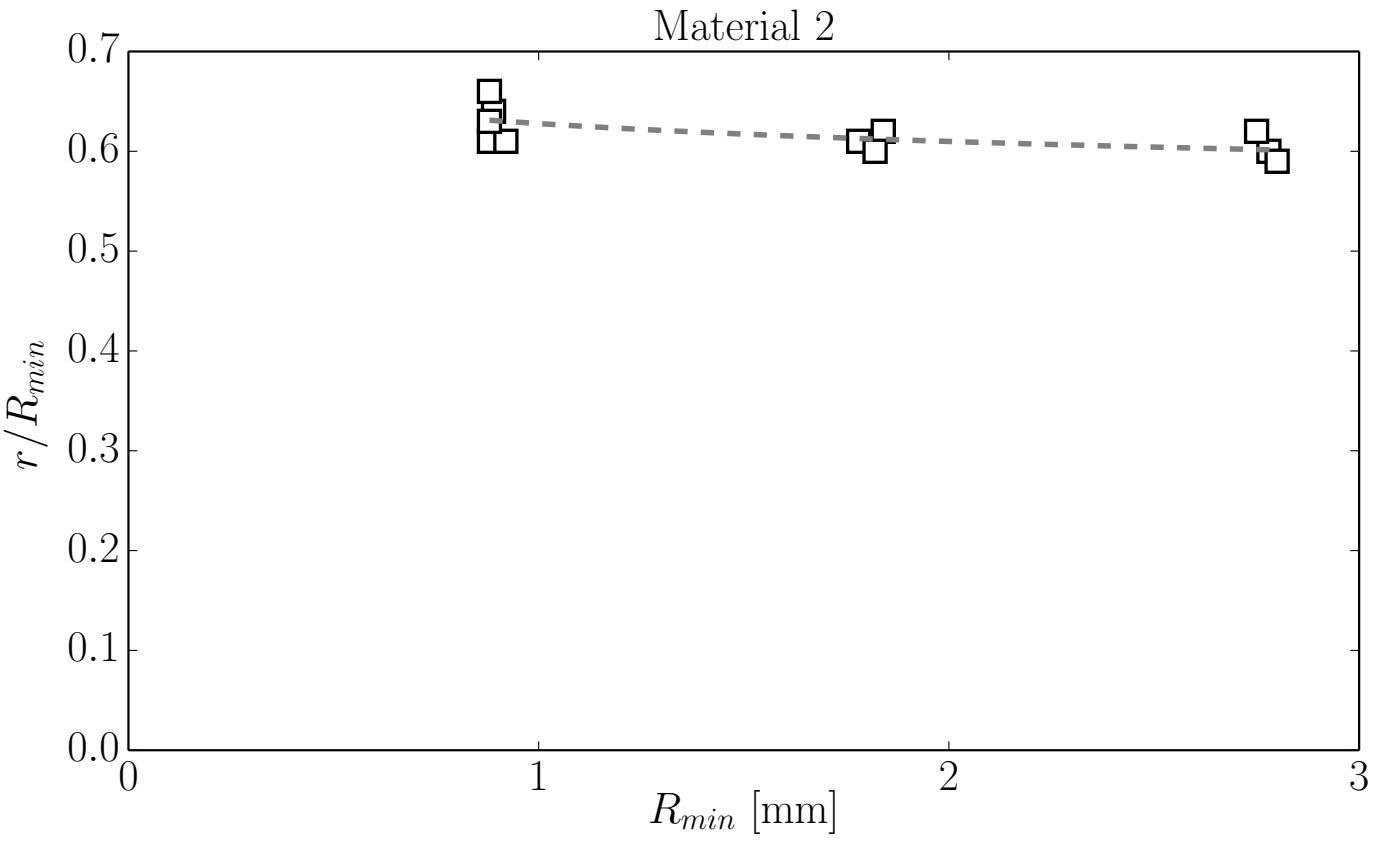

Figure 13
Click here to download high resolution image

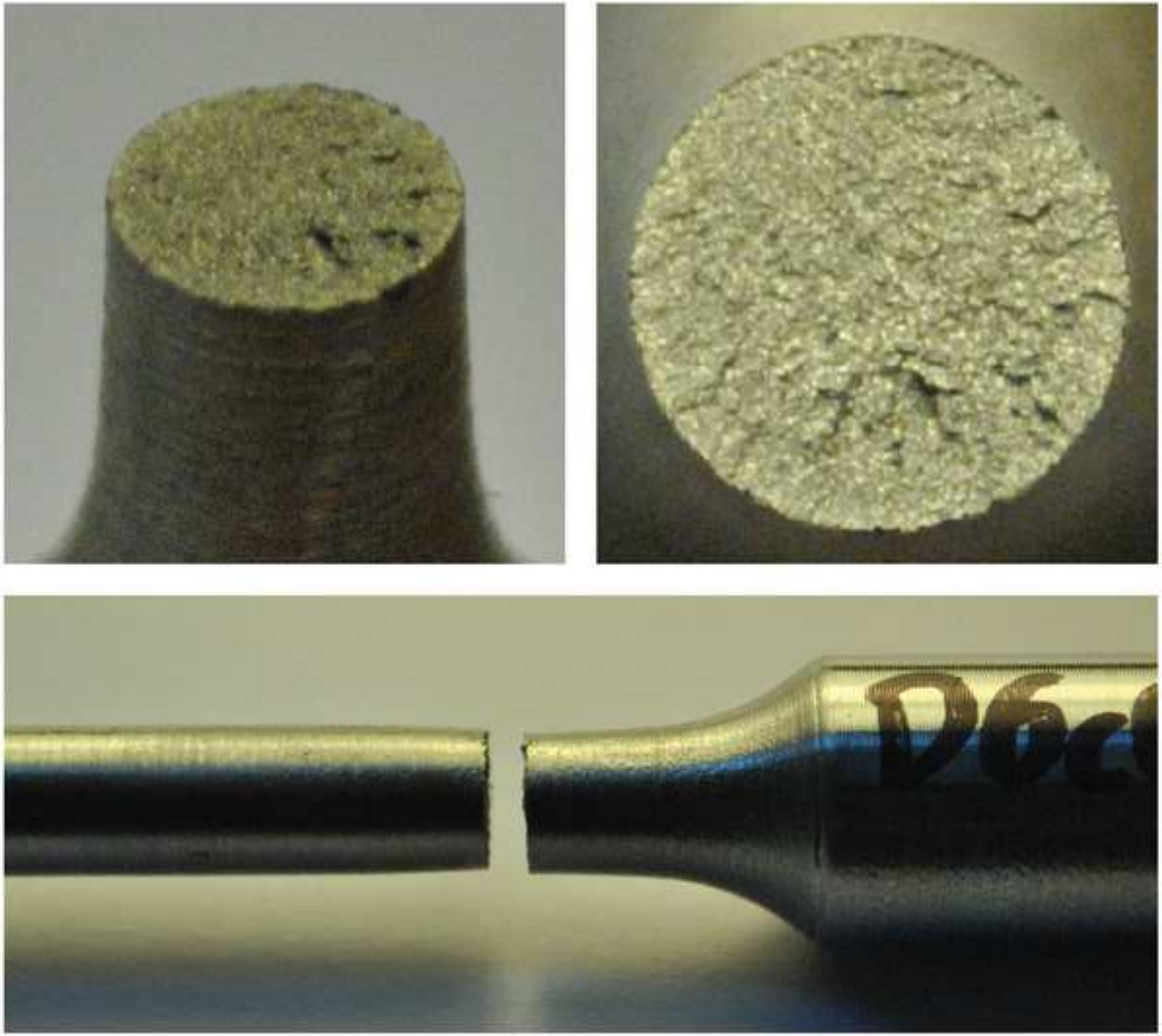

Figure 14
Click here to download high resolution image

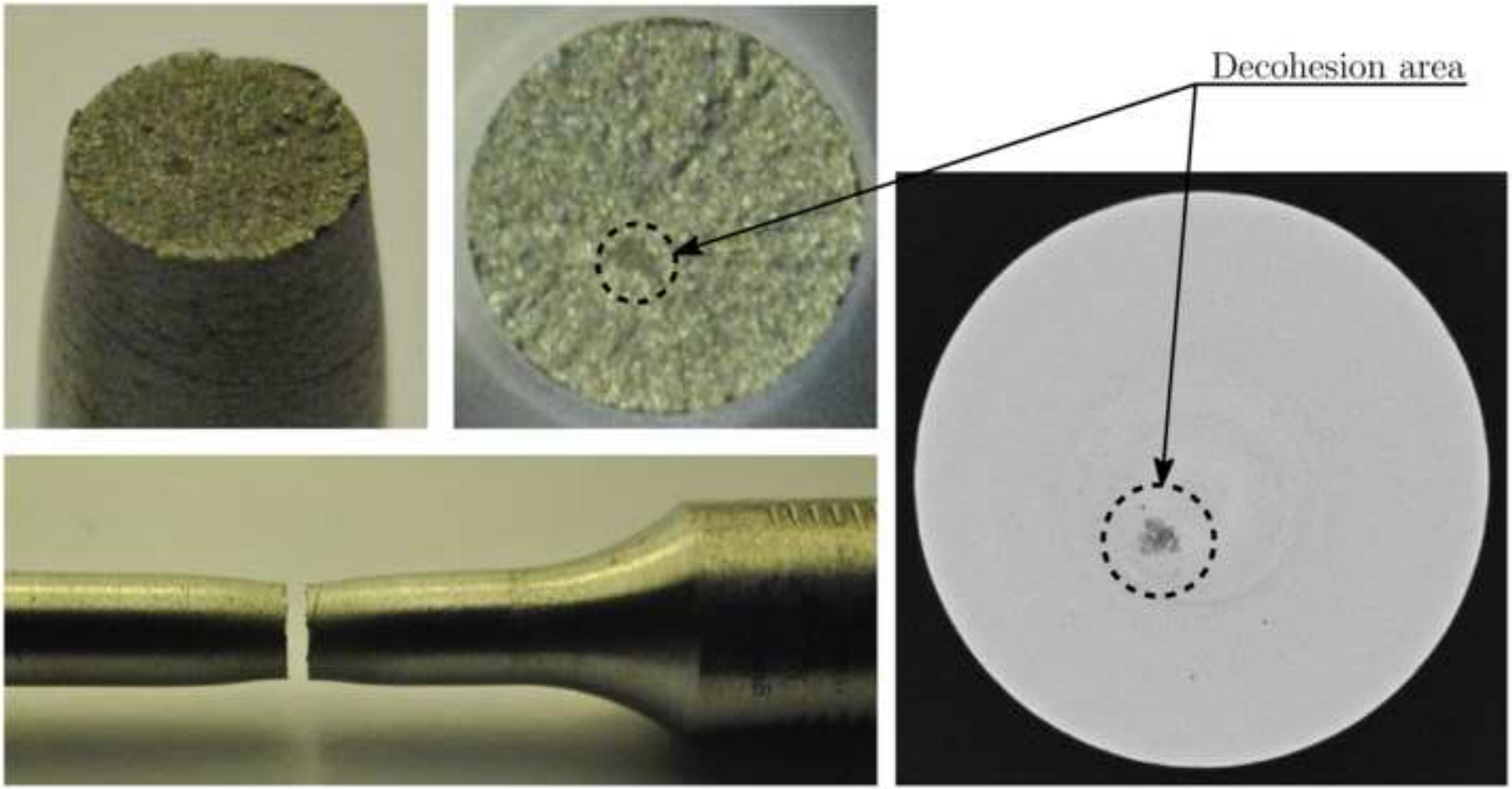

Figure 15
Click here to download high resolution image

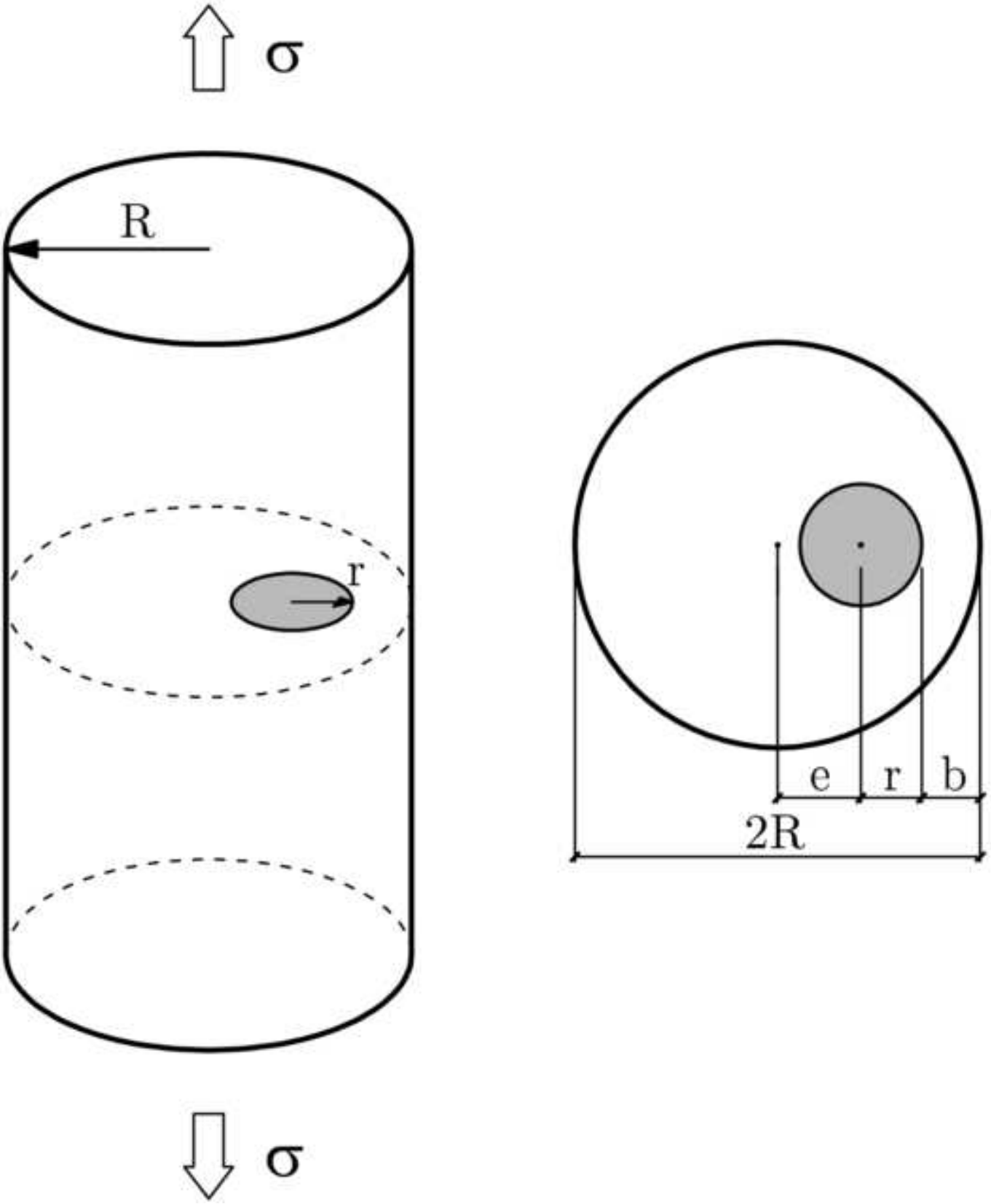

Figure 16

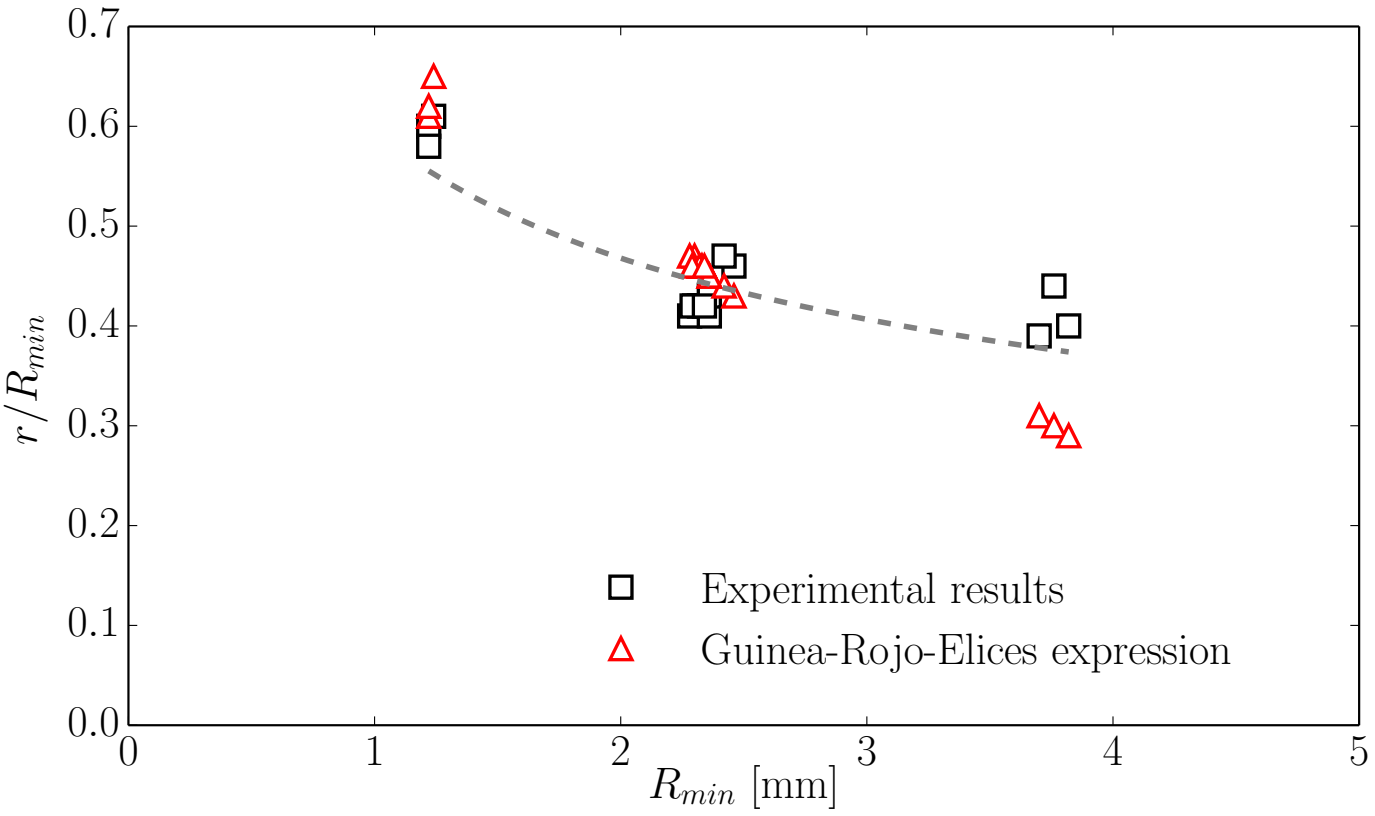
0.7
0.6
0.5
0.4
0.3
0.2
0.1
0.0
r/R_{min}
0
1
2
3
4
5
R_{min} [mm]
Experimental results
Guinea-Rojo-Elices expression